

AD-A260 153



①



National  
Defence      Défense  
                 nationale



# I/Q DEMODULATION OF RADAR SIGNALS WITH CALIBRATION AND FILTERING (U)

by

Jim P.Y. Lee

DTIC  
SELECTE  
JAN 29 1993  
S B D

**DISTRIBUTION STATEMENT A**  
Approved for public release  
Distribution Unlimited

98 1 28 040

**DEFENCE RESEARCH ESTABLISHMENT OTTAWA**  
REPORT NO. 1119

Canada

93-01670

December 1991  
Ottawa



6708



National    Défense  
Defence    nationale

# **I/Q DEMODULATION OF RADAR SIGNALS WITH CALIBRATION AND FILTERING (U)**

by

**Jim P.Y. Lee**  
*Radars ESM Section*  
*Electronic Warfare Division*

**DEFENCE RESEARCH ESTABLISHMENT OTTAWA**  
REPORT NO. 1119

PCN  
011LB

December 1991  
Ottawa

## ABSTRACT

A simple in-phase/quadrature (I/Q) demodulator architecture which can measure the amplitude, phase and instantaneous frequency of radar signals is examined in this report. This architecture has a potential for radar ESM applications where wide instantaneous bandwidth and simple algorithms for extracting the modulation characteristics of radar signals are required. This I/Q architecture can meet the requirement by splitting an incoming signal into its in-phase and quadrature components using analog hardware. However in practice, there are amplitude and phase imbalances between the two components and DC offsets, which can introduce large systematic errors in the measurements. In this report, we present novel techniques which can greatly reduce the systematic errors and improve the accuracy of the measurement. A time-domain analysis of the systematic errors is given. A calibration technique which can be used to correct for the imbalances and offsets is discussed. The effect of noise on the accuracy of the measurement is also examined. Imbalance errors and DC offsets of I/Q networks are measured and analyzed. Finally, a post-processing technique employing moving averages, which is shown to be effective for improving the output signal-to-noise ratio and reducing systematic errors, is also presented.

## RESUME

Une architecture de démodulateur à quadrature de phase pour la mesure de l'amplitude, de la phase et de la fréquence instantanée des signaux radar est examinée dans ce rapport. Cette architecture est prometteuse pour les applications de "mesures de soutien électronique radar" où une grande largeur de bande instantanée et des algorithmes simples permettant d'extraire la modulation des signaux radar sont requis. Cette architecture rencontre ces exigences en scindant, avec des composants analogiques, un signal d'entrée en ses deux composantes en quadrature de phase. Cependant des déséquilibres d'amplitude et de phase entre les deux composantes, ainsi que des biais de tension, peuvent en pratique introduire des erreurs systématiques assez grandes dans les mesures. Une analyse temporelle de ces erreurs systématiques est présentée. Une technique de calibration permettant de corriger les déséquilibres et les biais de tension est discutée. L'effet du bruit sur la précision des mesures est aussi examiné. Les erreurs dues aux déséquilibres et aux biais de tension dans les démodulateurs à quadrature sont mesurées et analysées. Enfin, une technique de filtrage qui permet de réduire les erreurs systématiques est présentée.

| Accession For       |                                     |
|---------------------|-------------------------------------|
| NTIS GRA&I          | <input checked="" type="checkbox"/> |
| DTIC TAB            | <input type="checkbox"/>            |
| Unannounced         | <input type="checkbox"/>            |
| Justification       |                                     |
| By _____            |                                     |
| Distribution/ _____ |                                     |
| Availability Codes  |                                     |
| Dist                | Avail and/or<br>Special             |
| A-1                 |                                     |

## EXECUTIVE SUMMARY

Due to the increasing density and complexity of radar signal waveforms, it is no longer easily possible to sort out uniquely and identify each radar emitter using conventional signal parameters such as pulse width, radio frequency (RF), amplitude and pulse repetition frequency. As a result there is a requirement for a radar Electronic Support Measures (ESM) receiver to measure the modulation characteristics of radar signals and to provide additional parameters which can be used to identify unambiguously each type of radar emitter. With the advent of fast A/D converters and high-speed digital signal processing technologies, it is possible to develop digital microwave receivers which can meet this requirement. A simple in-phase/quadrature (I/Q) demodulator architecture which can measure the amplitude, phase and instantaneous frequency of radar signals is examined in this report. The attractive features of this architecture for radar ESM applications are: (i) wide instantaneous bandwidth because the negative and positive frequencies with respect to the local oscillator frequency can be distinguished, and (ii) simple algorithms for the extraction of modulation characteristics can be used so that nearly real-time results can be obtained. However, because the splitting of the signal into its in-phase and quadrature components is implemented using analog components, there will be amplitude and phase imbalances between the two channels and DC offsets, which will introduce systematic errors to the measurement. Two techniques, compensation and low-pass filtering using a moving average, are proposed in this report for improving this simple architecture.

The effect of amplitude and phase imbalances and DC offsets is found to produce ripples on the measurement and the frequency of the ripples is harmonically related to the baseband frequency of the signal. For a given set of imbalance errors and DC offsets, the error introduced by the ripples on the instantaneous frequency is more severe and is directly proportional to the baseband frequency while the error is constant for both the amplitude and phase.

Some I/Q networks have been evaluated and the mean imbalance errors and DC offsets over a large frequency range can be large. In order to keep the systematic errors small, some form of compensation is needed to remove the mean errors and offsets. Once the mean errors and offsets are eliminated, the residual RMS errors as a function of frequency and input power level are quite small. If further improvement is required, calibration dependent on frequency and input power level may be needed.

The measurement accuracy on the amplitude, phase and instantaneous frequency has also been analyzed and given in terms of input SNR. For large input SNR, the standard deviation of the phase error decreases inversely proportional to the square root of the input SNR while the standard deviation of the envelope remains constant as the input signal level is varied.

There are two basic functions performed by using a moving average. The effective noise bandwidth of the I/Q network can be reduced with no appreciable degradation of the signal of interest, which will improve the output SNR. The ripples produced by the imbalance errors and DC offsets are usually outside the video bandwidth of the signal of

interest and thus can be reduced by low-pass filtering. In addition, a moving average is easy to implement digitally and does not introduce distortions such as ringing and overshoot.

Both the techniques of compensation and low-pass filtering using a moving average have been successfully demonstrated on the demodulation of pulsed and linear FM signals. They have been shown to be effective for improving the output signal-to-noise ratio and reducing systematic errors.

## TABLE OF CONTENTS

## PAGE

|  |     |
|--|-----|
| ABSTRACT/RESUME  | iii |
| EXECUTIVE SUMMARY  | v   |
| TABLE OF CONTENTS  | vii |
| LIST OF FIGURES  | ix  |
| <br>   |     |
| 1.0 INTRODUCTION   | 1   |
| 2.0 I/Q DEMODULATION   | 1   |
| 3.0 AMPLITUDE AND PHASE IMBALANCES AND DC OFFSETS                                | 3   |
| 3.1 Envelope Measurement   | 4   |
| 3.2 Phase and Frequency Measurement  | 4   |
| 4.0 COMPENSATION THROUGH CALIBRATION   | 10  |
| 5.0 SIGNAL PLUS NOISE  | 12  |
| 5.1 Phase Error As a Function of Signal-to-Noise Ratio                           | 12  |
| 5.2 Amplitude Error As a Function of Signal-to-Noise Ratio                       | 15  |
| 6.0 MOVING AVERAGE   | 16  |
| 7.0 EXPERIMENTAL MEASUREMENTS  | 17  |
| 7.1 Imbalance Errors and DC Offsets of I/Q Network                               | 17  |
| 7.2 Amplitude, Phase and Instantaneous Frequency Measurement<br>Versus Input SNR | 32  |
| 7.3 I/Q Demodulation of Signals  | 41  |
| 7.3.1 Pulse Modulated CW Signal  | 41  |
| 7.3.2 Linear FM Signal   | 50  |
| 8.0 SUMMARY AND CONCLUSIONS  | 50  |
| 9.0 REFERENCES   | 55  |

## LIST OF FIGURES

|              |  | <u>PAGE</u> |
|--------------|--|-------------|
| Figure 1     | Block Diagram of I/Q Sampling Network  | 2           |
| Figure 2     | Normalized Peak-to-Peak Ripple Versus Amplitude and Phase Imbalances                         | 5           |
| Figure 3     | Normalized Peak-to-Peak Ripple Versus DC Offsets   | 6           |
| Figure 4     | Maximum Instantaneous Frequency Deviation Versus Amplitude and Phase Imbalances              | 8           |
| Figure 5     | Maximum Instantaneous Frequency Deviation Versus DC Offsets                                  | 9           |
| Figure 6     | Functional Block Diagram of Compensation and Computation                                     | 13          |
| Figure 7     | Transfer Function of Moving Average (Single Layer)   | 18          |
| Figure 8     | Transfer Function of Moving Average (Two Layers)   | 19          |
| Figure 9     | Imbalance Errors and DC Offsets of I/Q Network ( Input Signal Power Level $\approx -19$ dBm) |             |
| Figure 9(a)  | Amplitude Ratio Versus Baseband Frequency  | 21          |
| Figure 9(b)  | Absolute Phase Difference Versus Baseband Frequency  | 22          |
| Figure 9(c)  | DC Offsets Versus Baseband Frequency   | 23          |
| Figure 9(d)  | Power Output Levels Versus Baseband Frequency  | 24          |
| Figure 10    | Imbalance Errors and DC Offsets of I/Q Network ( Input Signal Power Level $\approx -23$ dBm) |             |
| Figure 10(a) | Amplitude Ratio Versus Baseband Frequency  | 25          |
| Figure 10(b) | Absolute Phase Difference Versus Baseband Frequency  | 26          |
| Figure 10(c) | DC Offsets Versus Baseband Frequency   | 27          |
| Figure 10(d) | Power Output Levels Versus Baseband Frequency  | 28          |

LIST OF FIGURES (cont.)

|              |  | <u>PAGE</u> |
|--------------|--|-------------|
| Figure 11    | Imbalance Errors and DC Offsets of I/Q Network Versus Input Signal Level                                 |             |
| Figure 11(a) | Amplitude Ratio Versus Input Signal Level  | 29          |
| Figure 11(b) | Absolute Phase Difference Versus Input Signal Level  | 30          |
| Figure 11(c) | DC Offsets Versus Baseband Input Signal Level  | 31          |
| Figure 12    | RMS Phase Error Versus Input SNR   | 34          |
| Figure 13    | Ratio of RMS Amplitude Error to Mean Versus Input SNR  | 35          |
| Figure 14    | Normalized RMS Phase Difference Versus Input SNR<br>Using Experimental Data ( Noise Bandwidth = 20 MHz ) | 36          |
| Figure 15    | Normalized Cross-Covariance Versus Input SNR<br>Using Experimental Data ( Noise Bandwidth = 20 MHz )     | 37          |
| Figure 16    | Normalized RMS Phase Difference Versus Input SNR<br>Using Simulated Data ( Noise Bandwidth = 20 MHz )    | 38          |
| Figure 17    | Normalized Cross-Covariance Versus Input SNR<br>Using Simulated Data ( Noise Bandwidth = 20 MHz )        | 40          |
| Figure 18    | Normalized RMS Phase Difference Versus Input SNR<br>Using Simulated Data ( Noise Bandwidth = 40 MHz )    | 42          |
| Figure 19    | Normalized Cross-Covariance Versus Input SNR<br>Using Simulated Data ( Noise Bandwidth = 40 MHz )        | 43          |
| Figure 20    | Envelope of a 0.5- $\mu$ s Pulse<br>(Baseband Frequency = 40 MHz and $T_s = 10$ ns)                      |             |
| Figure 20(a) | Raw Data   | 44          |
| Figure 20(b) | After a 7-point Moving Average   | 45          |
| Figure 20(c) | After Compensation and 3-point Moving Average  | 46          |

LIST OF FIGURES (cont.)

|              |   | <u>PAGE</u> |
|--------------|---|-------------|
| Figure 21    | Instantaneous Frequency of a 0.5- $\mu$ s Pulse<br>(Baseband Frequency = 40 MHz and $T_s = 10$ ns)  |             |
| Figure 21(a) | Raw Data  | 47          |
| Figure 21(b) | After Compensation  | 48          |
| Figure 21(c) | After Compensation and 3-point Moving Average   | 49          |
| Figure 22    | Envelope of a Linear FM Pulse<br>( Pulse Width = 0.5 $\mu$ s, Center Frequency = 40 MHz,<br>$\Delta f = 10$ MHz and $T_s = 10$ ns)                |             |
| Figure 22(a) | Raw Data  | 51          |
| Figure 22(b) | After Compensation and 5-point Moving Average   | 52          |
| Figure 23    | Instantaneous Frequency of a Linear FM Pulse<br>( Pulse Width = 0.5 $\mu$ s, Center Frequency = 40 MHz,<br>$\Delta f = 10$ MHz and $T_s = 10$ ns) |             |
| Figure 23(a) | Raw Data  | 53          |
| Figure 23(b) | After Compensation and 5-point Moving Average   | 54          |

## 1.0 INTRODUCTION

Due to the increasing density and complexity of radar signal waveforms, it is no longer easily possible to sort out uniquely and identify each radar emitter using conventional signal parameters such as pulse width, radio frequency (RF), amplitude and pulse repetition frequency. As a result there is a requirement for a radar Electronic Support Measures (ESM) receiver to measure the modulation characteristics of radar signals and to provide additional parameters which can be used to identify unambiguously each type of radar emitter. With the advent of fast A/D converters and high-speed digital signal processing technologies, it is possible to develop digital microwave receivers which can meet this requirement [1]. A simple in-phase/quadrature (I/Q) demodulator architecture which can measure the amplitude, phase and instantaneous frequency of radar signals is shown in Fig. 1. The attractive features of this architecture for radar ESM applications are: (i) wide instantaneous bandwidth because the negative and positive frequencies with respect to the local oscillator frequency can be distinguished, and (ii) simple algorithms for the extraction of modulation characteristics can be used so that nearly real-time results can be obtained. However, because the splitting of the signal into its in-phase and quadrature components is implemented using analog components, there will be amplitude and phase imbalances between the two channels and DC offsets, which will introduce systematic errors to the measurement[2-3].

This report addresses this I/Q sampling architecture for the measurement of amplitude, phase and instantaneous frequency of radar signals. A time-domain analysis, on the effects of phase and amplitude imbalances between the I and Q channels and DC offsets, is given. A calibration technique which can be used to compensate for the imbalances and offsets is discussed. The effect of noise on the measurement is analyzed. Imbalance errors and DC offsets of I/Q networks are measured and analyzed. Finally, a post-processing technique employing moving averages, which can be used for improving the output signal-to-noise ratio and reducing systematic errors, is also presented.

## 2.0 I/Q DEMODULATION

An incoming RF signal is usually down-converted to an intermediate signal (IF) before it is applied to the I/Q network. The IF signal to the I/Q demodulator, as shown in Fig. 1, can be expressed in the form of

$$s(t) = a(t)\cos[\omega_0 t + \phi(t)] \quad (1)$$

where  $a(t)$  is the amplitude or envelope,  $\omega_0$  is the angular carrier frequency and  $\phi(t)$  is the phase function of the signal. It is first bandpass filtered and then equally power-divided into two paths. The signal in each path is then mixed down to baseband by the use of a local oscillator signal. The two local oscillator signals are derived from the same source, but are 90 degrees out of phase. The resultant in-phase and quadrature baseband signals after the low-pass filter (LPF) are,

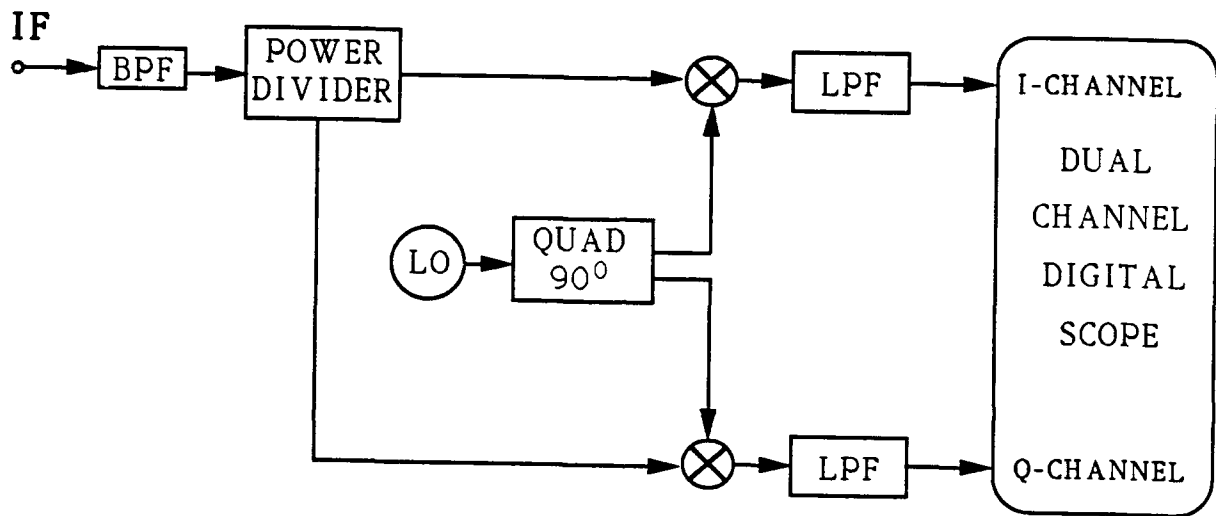


Fig. 1 Block Diagram of I/Q Sampling Network

$$S_i(t) = K/2 a(t)\cos[ (\omega_o - \omega_{1o})t + \phi(t) - \gamma ] = K/2 a(t)\cos[\beta(t)] \quad (2)$$

and

$$S_q(t) = K/2 a(t)\sin[\beta(t)] \quad (3)$$

respectively, where  $K$  is the net gain in each path,  $\omega_{1o}$  is the angular frequency of the local oscillator with initial phase  $\gamma$ ,  $\beta(t)$  is the phase function of the baseband signal and a constant delay introduced in each path has been neglected. In this ideal case, the two channels have been assumed to be perfectly matched in amplitude, 90 degrees out of phase and with no DC offsets.

The instantaneous power of the envelope of the input signal is simply related to its in-phase and quadrature baseband components by

$$a^2(t) = 4/K^2 [ S_i^2(t) + S_q^2(t) ], \quad (4)$$

the signal phase function is given by

$$\begin{aligned} \phi(t) &= \beta(t) - (\omega_o - \omega_{1o})t + \gamma \\ &= \tan^{-1} [S_q(t)/S_i(t)] - (\omega_o - \omega_{1o})t + \gamma \end{aligned} \quad (5)$$

and the instantaneous angular frequency is

$$2\pi f(t) = \frac{d\phi(t)}{dt} = \frac{d}{dt} \left[ \tan^{-1} [S_q(t)/S_i(t)] \right] - (\omega_o - \omega_{1o}). \quad (6)$$

The in-phase and quadrature baseband signals are usually sampled and digitized at  $t_n = nT_s + T_o$ , where  $T_s$  is the sampling interval,  $T_o$  is the initial time and  $n = 0, 1, 2, \dots$ . In this case, the sampled instantaneous angular frequency is then approximately given by

$$2\pi f(t_n) \approx \left[ \phi(t_n) - \phi(t_{n-1}) \right] / T_s \quad (7)$$

### 3.0 AMPLITUDE AND PHASE IMBALANCES AND DC OFFSETS

In the implementation of the I/Q network, there will be differential gain, DC offsets and phase deviation from the ideal 90 degrees between the two channels [3]. Equations (2) and (3) can then be rewritten in a more general form as

$$S_i(t) = K_i/2 a(t)\cos[\beta(t) + \phi_i] + a_{i0} \quad (8)$$

and

$$S_q(t) = K_q/2 a(t)\sin[\beta(t) + \phi_q] + a_{q0} \quad (9)$$

respectively, where  $a_{i0}$  and  $a_{q0}$  are the amplitude DC offsets,  $K_i$  and  $K_q$  are the gains, and

$\phi_i$  and  $\phi_q$  are the phases of the in-phase and quadrature channels respectively.  $a_{i0}$ ,  $a_{q0}$ ,  $K_i$ ,  $K_q$ ,  $\phi_i$  and  $\phi_q$  are in general a function of frequency. For narrow-band signals, they can be assumed to be approximately constant.

### 3.1 Envelope Measurement

Substituting Eqs.(8) and (9) into Eq.(4), the instantaneous power of the envelope of the baseband signal can be shown to be [4]

$$\begin{aligned}
 S_i^2(t) + S_q^2(t) = [a(t)K_i]^2/4 \left\{ 1/2 + \{a_{i0}/[a(t)K_i/2]\}^2 + R^2/2 + \{a_{q0}/[a(t)K_i/2]\}^2 \right. \\
 + \left[ \cos[\beta(t) + \phi_i] \{2 a_{i0}/[a(t)K_i/2] + 2 R a_{q0}/[a(t)K_i/2] \sin[(\phi_q - \phi_i)]\} \right. \\
 + \left. \left. 2 R a_{q0}/[a(t)K_i/2] \sin[\beta(t) + \phi_i] \cos[(\phi_q - \phi_i)] \right] \right. \\
 \left. + 1/2 \cos \{ 2 [\beta(t) + \phi_i] \} - R^2/2 \left[ \cos \{ 2 [\beta(t) + \phi_i] + [ 2 (\phi_q - \phi_i) ] \} \right] \right\} \quad (10)
 \end{aligned}$$

The envelope has been expressed in terms of normalized parameters, i.e., (i) amplitude imbalance ratio ( $R = K_q/K_i$ ), (ii) phase imbalance ( $\phi_q - \phi_i$ ), and (iii) normalized DC offsets  $a_{i0}/[a(t)K_i/2]$  and  $a_{q0}/[a(t)K_i/2]$  of the in-phase and quadrature channels respectively. If the envelope of the input signal  $[a(t)]$  is constant, then there are basically three groups of terms inside the braces; DC terms, fundamental baseband frequency terms and second harmonic baseband frequency terms. The DC terms is a function of the amplitude imbalance and DC offsets, independent of phase imbalance. A DC offset will introduce a fundamental harmonic frequency which has the same frequency as the baseband signal. Other errors will only affect the magnitude of these ripples. Without DC offsets, ripples of the fundamental frequency will disappear completely. Ripples with a second harmonic frequency will appear only when there is an amplitude or phase imbalance. When the two channels are matched, all the ripples will disappear and the terms inside the brackets will be unity. The effects of the three different sources of errors on the measurement have been analyzed in detail [4]. The ratios of the peak-to-peak ripple to the mean are plotted in Figs.2 and 3, for the cases when there are only amplitude and phase imbalances, and when there are only DC offsets respectively. When there are only amplitude and phase imbalances in the network, the ratio of peak-to-peak ripple to mean is a function of the absolute phase imbalance and the amplitude imbalance ratio expressed in dB. In the case, when there are only DC offset errors, the ratio is just a function of the absolute value of the normalized DC offsets.

### 3.2 Phase and Frequency Measurement

Substituting Eqs.(8) and (9) into Eq.(5), results in the phase of the baseband signal given by

$$\begin{aligned}
 \alpha(t) = \tan^{-1} \left\{ R \left[ \sin[\beta(t) + \phi_i] \cos[(\phi_q - \phi_i)] + \cos[\beta(t) + \phi_i] \right. \right. \\
 \left. \left. \cdot \sin[(\phi_q - \phi_i)] + a_{q0}/[a(t)K_q/2] \right] / \left[ \cos[\beta(t) + \phi_i] + a_{i0}/[a(t)K_i/2] \right] \right\} \quad (11)
 \end{aligned}$$

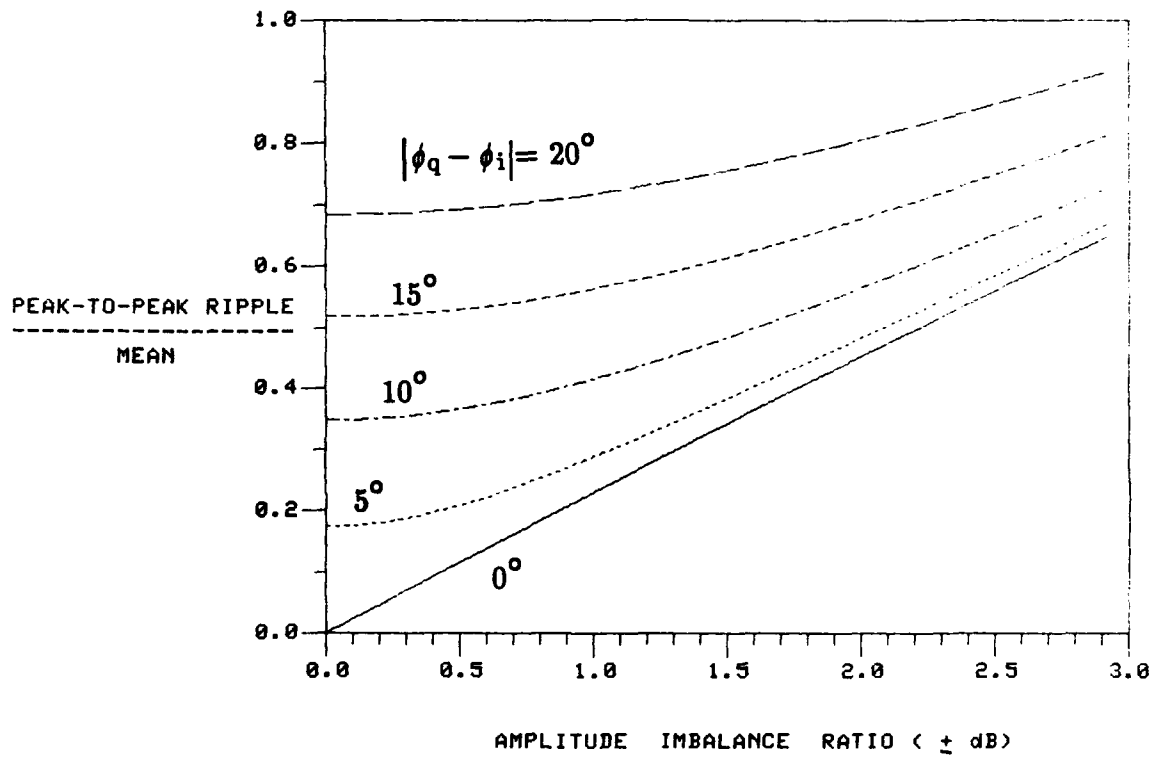


Fig. 2 Normalized Peak-to-Peak Ripple Versus Amplitude and Phase Imbalances

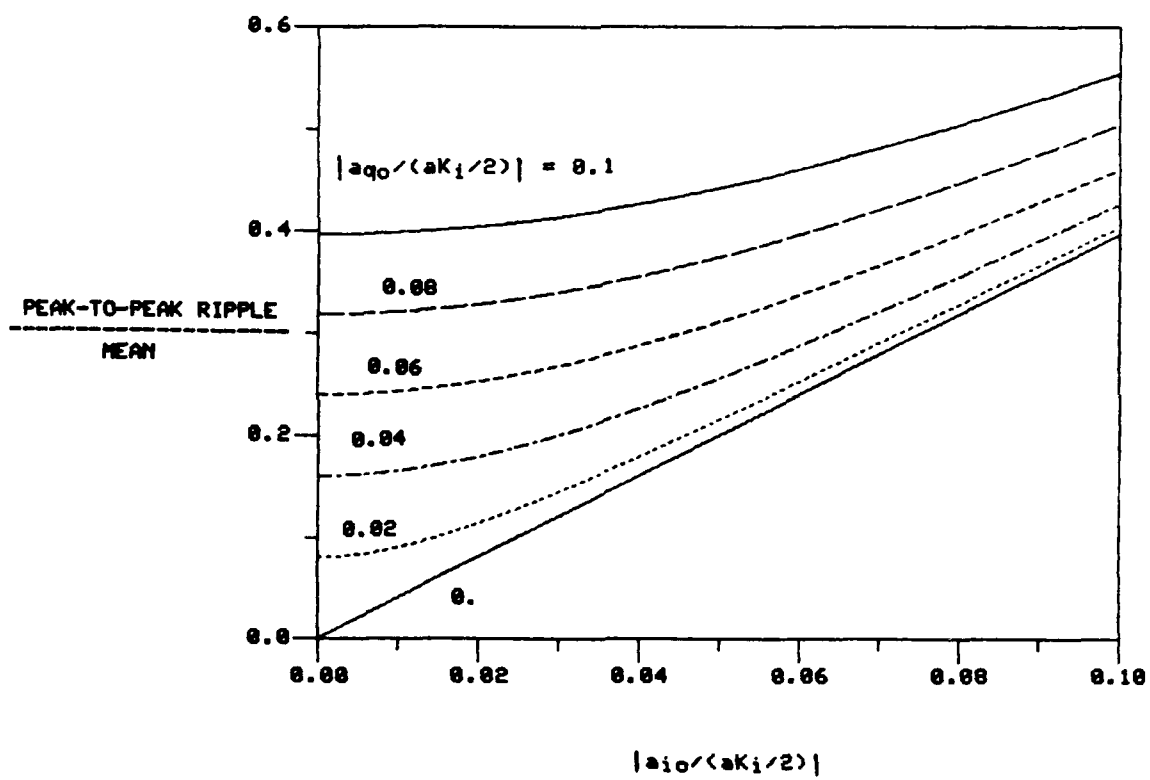


Fig. 3 Normalized Peak-to-Peak Ripple Versus DC Offsets

where the argument has also been expressed in terms of normalized parameters.

The deviation in measurement from the case of an ideal sampling network is emphasized in this analysis. The phase error is defined by the difference between the measured phase function and the input phase function of the baseband signal as

$$\Delta a(t) = a(t) - a_o(t) \quad (12)$$

where

$$a_o(t) = \beta(t) + \phi_i \quad (13)$$

is the input phase function of the baseband signal with a constant phase offset  $\phi_i$ . For a specific set of imbalance errors and DC offsets, the phase error can be fully characterized by plotting  $\Delta a(t)$  over an input phase change of  $2\pi$  radians [4]. The measured phase value  $[a(t)]$  is then obtained from Eq.(12) once the phase function of the input signal is known. It is to be noted that the imbalance errors and DC offsets are usually a function of frequency. The measured frequency deviation from the input baseband signal is then obtained by differentiating Eq.(12) with respect to time

$$\frac{\partial[\Delta a(t)]}{\partial t} = \frac{\partial[\Delta a(t)]}{\partial[a_o(t)]} \frac{\partial[a_o(t)]}{\partial t} \quad (14)$$

where  $\partial[\Delta a(t)]/\partial[a_o(t)]$  is the partial derivative of the measured phase change with respect to the input phase and is dimensionless. It is also a very useful parameter in characterizing the normalized frequency deviation due to the imbalance errors and DC offsets. It is found that the imbalance errors and DC offsets have a similar effect on both the measured phase and instantaneous frequency as in the case of the measured envelope [4]. The major difference is that the ripples generated are more complex in shape. Figure 4 shows the normalized maximum positive and maximum negative frequency deviations as a function of the amplitude and phase imbalances while Fig. 5 shows the frequency deviation due to DC offsets only. In Fig. 4, the maximum normalized frequency deviation is only a function of the absolute phase imbalance and similarly in Fig. 5, it is only a function of the absolute value of the DC offset.

For a given set of imbalance errors and DC offsets, the normalized peak frequency deviations are completely determined by a plot of  $\partial[\Delta a(t)]/\partial[a_o(t)]$  over an input phase change of  $2\pi$  radians. The measured maximum frequency deviations from the input signal is determined by multiplying the normalized peak frequency deviations by the instantaneous frequency of the input signal at the baseband frequency as given in Eq.(14). If the imbalance errors and DC offsets are about the same as a function of IF frequency, the measured frequency error due to the ripples can be minimized by choosing an IF signal which gives the lowest baseband frequency.

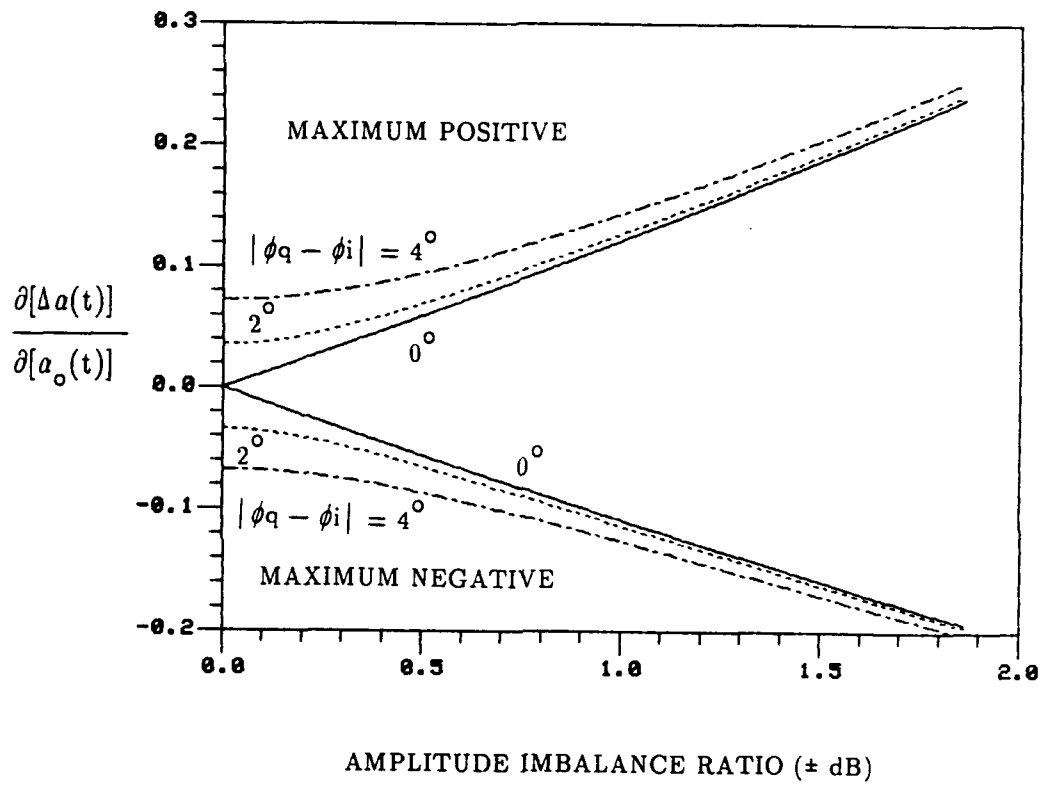


Fig. 4 Maximum Instantaneous Frequency Deviation Versus Amplitude and Phase Imbalances

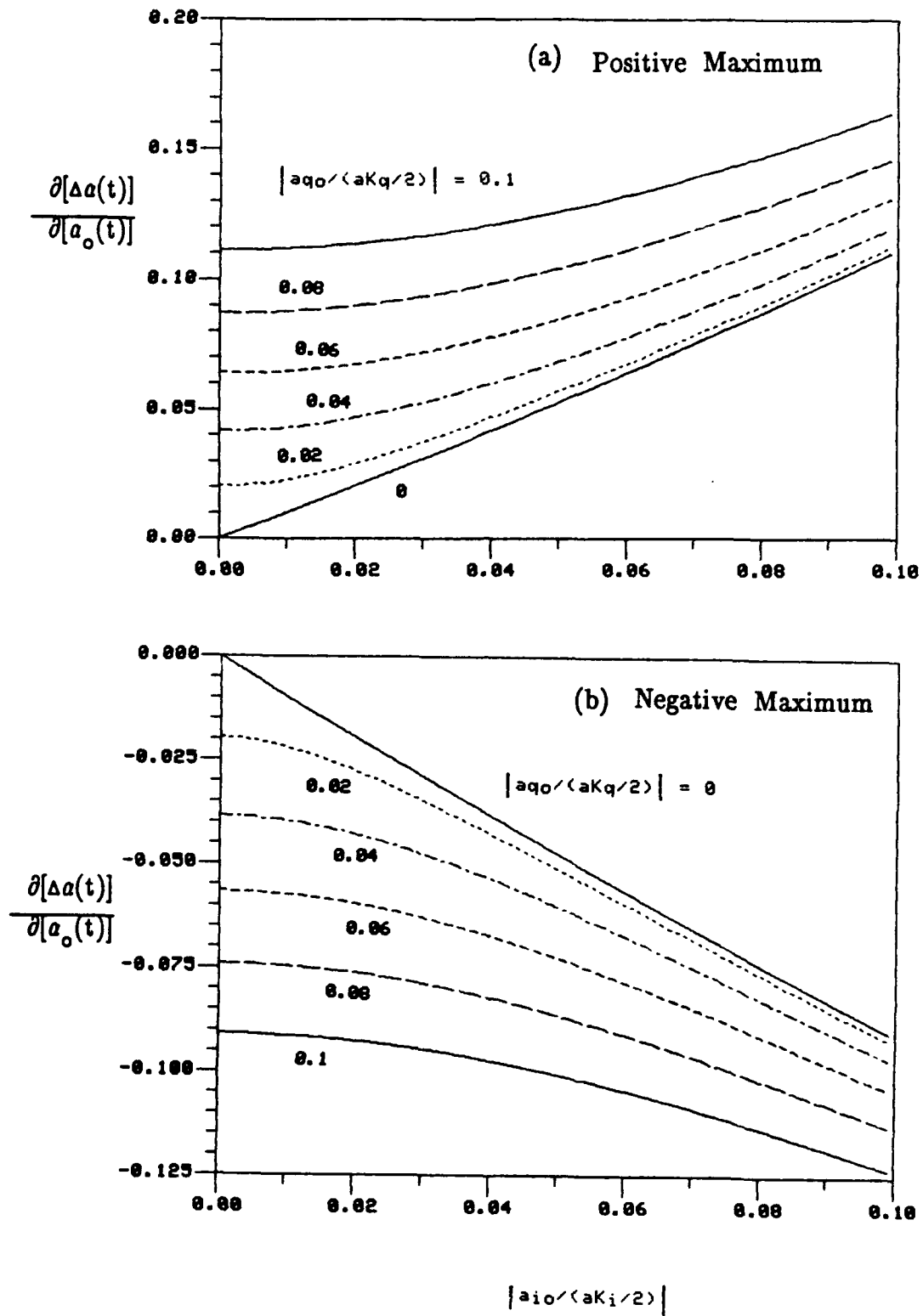


Fig. 5 Maximum Instantaneous Frequency Deviation Versus DC Offsets

#### 4.0 COMPENSATION THROUGH CALIBRATION

Since most of the imbalance errors and DC offsets are stationary and are only a function of frequency, some compensation can be carried out to eliminate them. When a calibration signal of the form given by Eq.(1) is applied to the I/Q network, the resultant in-phase and quadrature baseband signals are given by Eqs. (8) and (9) respectively. When the sine function of the baseband signal in the quadrature channel is expressed in terms of a cosine function and the phase imbalance, Eq.(9) can be rewritten as

$$\begin{aligned} S_q(t) &= K_q/2 a(t)\sin[\beta(t) + \phi_q] + a_{q0} \\ &= a(t) K_q/2 \left[ \cos [\beta(t) + \phi_i - \pi/4] \cos[(\phi_q - \phi_i)] \right. \\ &\quad \left. + \cos [\beta(t) + \phi_i] \sin[(\phi_q - \phi_i)] \right] + a_{q0} \end{aligned} \quad (15)$$

Taking the Fourier transform of the above expression over a finite duration T, we have

$$\begin{aligned} \mathcal{F}[S_q(t)] &= K_q/2 \cos[(\phi_q - \phi_i)] \exp(-j\pi/4) \mathcal{F}\left[ a(t)\cos [\beta(t) + \phi_i] \right] \\ &\quad + K_q/2 \sin[(\phi_q - \phi_i)] \mathcal{F}\left[ a(t)\cos [\beta(t) + \phi_i] \right] + \mathcal{F}[a_{q0}] \\ &= -jK_q/2 \exp[j(\phi_q - \phi_i)] \mathcal{F}\left[ a(t)\cos [\beta(t) + \phi_i] \right] + \mathcal{F}[a_{q0}] \end{aligned} \quad (16)$$

$$\text{where } \mathcal{F}[h(t)] = \int_{-T/2}^{T/2} h(t) \exp(-j2\pi ft) dt \quad (17)$$

is the finite Fourier transform. For a given baseband signal, the time duration T must be chosen so that there will be negligible overlapping between the frequency spectrum of the signal and the spectrum of the truncated DC offset.

The Fourier transform of the in-phase component is

$$\mathcal{F}[S_i(t)] = K_i/2 \mathcal{F}\left[ a(t) \cos[\beta(t) + \phi_i] \right] + \mathcal{F}[a_{i0}] \quad (18)$$

The DC frequency component due to the DC offset can be separated and removed if there is negligible overlapping between the frequency components generated by the truncated DC offset and those due to the signal. The DC offsets of the in-phase and quadrature channels are simply related to its finite Fourier transform by

$$a_{i0} = \left[ \mathcal{F}[a_{i0}] \text{ at } f = 0 \right] / T \quad (19)$$

and

$$a_{q0} = \left[ \mathcal{F}[a_{q0}] \text{ at } f = 0 \right] / T \quad (20)$$

respectively. Taking the ratio of the Fourier transform of the signal in the quadrature channel to the Fourier transform of the signal in the in-phase channel, we have

$$\begin{aligned} \mathcal{F}[S_q(t)] / \mathcal{F}[S_i(t)] &= -j \exp[j(\phi_q - \phi_i)] K_q / K_i \\ &= R \exp \left[ j[(\phi_q - \phi_i) - \pi/4] \right] \end{aligned} \quad (21)$$

Once the ratio of  $\mathcal{F}[S_q(t)] / \mathcal{F}[S_i(t)]$  is computed, the relative amplitude imbalance ratio  $R$  and the phase imbalance  $(\phi_q - \phi_i)$  as a function of frequency can then be determined. Using the above procedure and knowing the input IF frequency, all the imbalance errors and DC offsets of the network can be measured.

In practice, the baseband signals are sampled and digitized. As a result, a discrete Fourier transform (DFT) has to be used and  $t$  is replaced by  $t_n$ . Moreover, a CW calibration signal is used for two main reasons: (i) precise CW sources are readily available and (ii) the number of data samples generated at a particular frequency of interest can be arbitrarily large. A large number of data samples for the DFT can improve the output signal-to-noise ratio and thus the ultimate accuracy of the measurement. Since both the input IF frequency and the resultant baseband frequency are known, the number of sample points can also be chosen to satisfy the criterion of having a truncation interval for the DFT equal to an integer multiple of the period of the baseband signal. Once this criterion is satisfied, the leakage problem due to time domain truncation associated with DFT can be eliminated [5]. This is due to the fact that when the truncation interval is equal to an integer multiple of the period of the baseband signal, the CW signal will locate at one of the nulls of the Fourier transformed sinc function. As a result, no distortions are introduced to either the CW signal or the DC offset. The DC offset is determined by dividing the DC component of the DFT by the total number of sample points used.

Once the imbalance errors and DC offsets as a function of frequency are known the errors can be eliminated by a calibration technique. In the simplest case where the imbalance errors and DC offsets of the I/Q network over the signal bandwidth are approximately constant, a single set of calibration values can be applied to every data point once the approximate frequency of the signal is estimated.

Recall that the objective is to obtain  $a_o(t)$  in Eq.(13). For this we need expressions for  $a(t)\sin[\beta(t) + \phi_i]$  and  $a(t)\cos[\beta(t) + \phi_i]$ . Using both Eqs.(8) and (9),  $a(t)\sin[\beta(t) + \phi_i]$  can be expressed in terms of the measured baseband signals, and the imbalance errors and DC offsets as

$$\begin{aligned} a(t)\sin[\beta(t) + \phi_i] &= \left[ [S_q(t) - a_{q0}] / (K_q/2) - [S_i(t) - a_{i0}] / (K_i/2) \right. \\ &\quad \left. \cdot \sin[(\phi_q - \phi_i)] \right] / \cos[(\phi_q - \phi_i)] \end{aligned} \quad (22)$$

Similarly, from Eq.(18), we also have

$$a(t) \cos[\beta(t) + \phi_i] = [S_i(t) - a_{i0}]/(K_i/2) \quad (23)$$

Dividing Eq.(22) by Eq.(23) and taking the arctangent of the ratio, the phase function of the compensated baseband signal is given by

$$\begin{aligned} [\beta(t) + \phi_i] &= \alpha_o(t) \\ &= \tan^{-1} \left\{ \frac{[S_q(t) - a_{q0}]/R - [S_i(t) - a_{i0}] \sin[(\phi_q - \phi_i)]}{[\cos[(\phi_q - \phi_i)] [S_i(t) - a_{i0}]]} \right\} \end{aligned} \quad (24)$$

Since the compensated phase function of the baseband signal is known, the compensated amplitude of the envelope is obtained by using Eq.(23). Hence

$$a(t) = 2/K_i [S_i(t) - a_{i0}]/\cos[\beta(t) + \phi_i] \quad (25)$$

A functional block diagram for the above compensation and computation process is shown in Fig. 6.

The next section considers the effect of input noise on the measurements.

## 5.0 SIGNAL PLUS NOISE

In radar ESM applications, the intercepted radar signal is usually amplified by a pre-amplifier at the RF and then down-converted to an IF signal. The IF signal is then amplified again before it is applied to the input of the I/Q network. The input noise contribution is usually dominated by the RF front-end pre-amplifier noise since subsequent stages in the receiver are preceded by sufficient gain in order to overcome additional noise. The active components in the I/Q network will also introduce noise. In addition, quantization noise will also be introduced when the baseband signals are digitized. It is assumed that the RF noise is dominant and is white Gaussian with zero mean and spectral density  $\eta/2$  at the input of the I/Q network. After mixing down to baseband and with low pass filtering, the noise in the two channels are uncorrelated with each having a spectral density  $K^2\eta/4$ . For  $B_{IF} = 2 B_{LP}$ , where  $B_{LP}$  is the LPF bandwidth, and if the signal is approximately located at the center of the band pass filter (BPF), the mean signal-to-noise ratio (SNR) at the output of each channel is about the same as that at the input. The signals in both the in-phase and quadrature channels are of equal peak amplitude  $[Ka(t)/2]$ . The mean SNR  $[a^2(t)/(2\sigma^2)]$  in each channel is equal to  $a^2(t)/(4\eta B_{LP})$ .

### 5.1 Phase Error As a Function of Signal-to-Noise Ratio

At time  $t = t_o$ , when the phase of the input signal  $\theta_o = \beta(t_o)$ , the probability

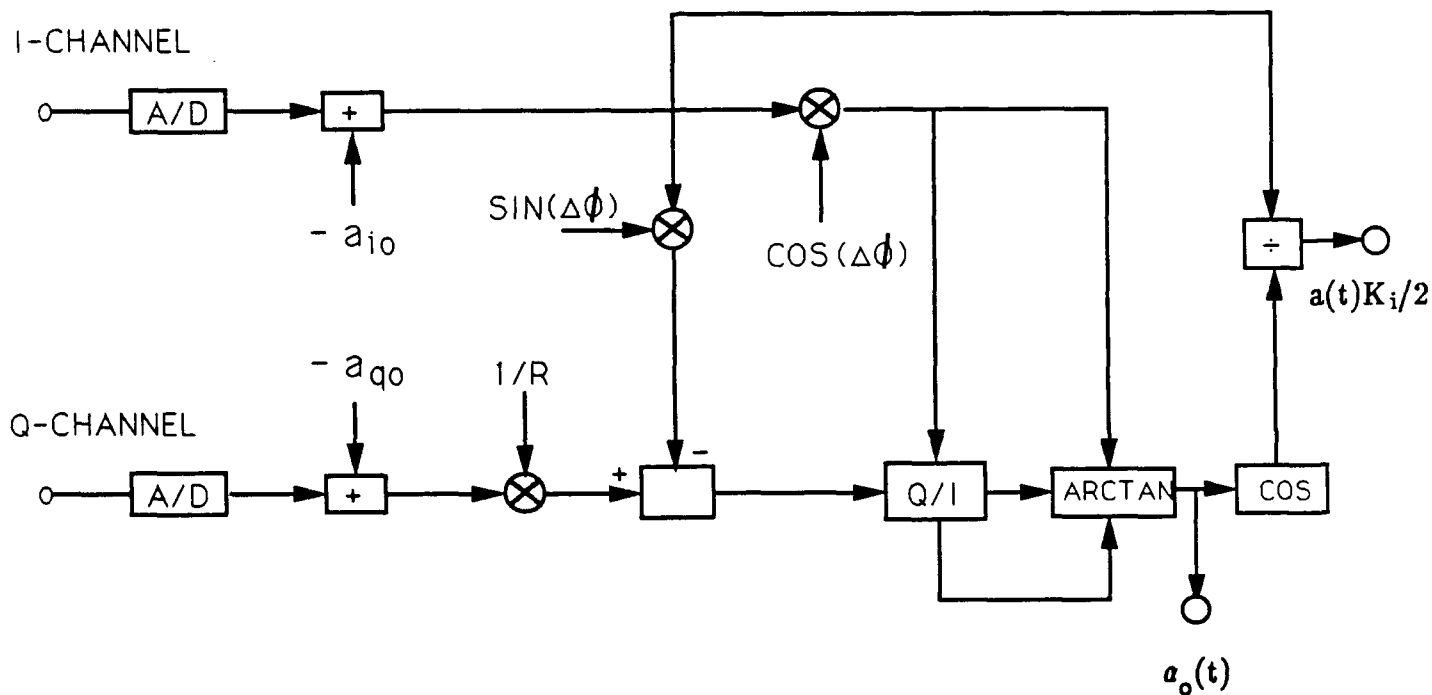


Fig. 6 Functional Block Diagram of Compensation and Computation

density function as a function of SNR can be shown to be [4,6]

$$f_{\theta_o}(\theta) = 1/(2\pi) \exp[-\text{SNR}] + (\text{SNR})^{1/2} \cos(\theta - \theta_o) / [2(\pi)^{1/2}] \cdot \exp \left[ -\text{SNR} [\sin(\theta - \theta_o)]^2 \right] \cdot \left[ 1 + \text{erf}[(\text{SNR})^{1/2} \cos(\theta - \theta_o)] \right], \text{ for } |\theta| \leq \pi \quad (26)$$

where

$$\text{erf}(x) = 2/\sqrt{\pi} \int_0^x \exp(-t^2) dt \quad (27)$$

For small SNR ratios, the second term is negligible and the probability function is approximately given by

$$f_{\theta_o}(\theta) \approx 1/(2\pi), \text{ for } |\theta| \leq \pi \quad (28)$$

which is uniform in distribution. For large SNR ratios, the first term is negligible and

$$\begin{aligned} \text{erf}[(\text{SNR})^{1/2} \cos(\theta - \theta_o)] &\approx 1 \\ \cos(\theta - \theta_o) &\approx 1 \text{ and} \\ \sin(\theta - \theta_o) &\approx \theta - \theta_o \end{aligned} \quad (29)$$

Substituting the above approximations into Eq.(26), we have

$$\begin{aligned} f_{\theta_o}(\theta) &\approx (\text{SNR})^{1/2} / (\pi)^{1/2} \exp[-\text{SNR}(\theta - \theta_o)^2], \text{ for } |\theta| \leq \pi \\ \text{or} &\approx 1 / [(2\pi)^{1/2} \sigma / a(t_o)] \exp \left[ -(\theta - \theta_o)^2 / \{2[\sigma / a(t_o)]^2\} \right], \text{ for } |\theta| \leq \pi \end{aligned} \quad (30)$$

which is approximately Gaussian.

Once  $f_{\theta_o}(\theta)$  is determined, the mean and variance of the measured phase angle can easily be determined by using the following equations:

$$E(\theta_o) = \eta_{\theta_o} = \int_{-\infty}^{\infty} \theta f_{\theta_o}(\theta) d\theta, \text{ where } |\theta| \leq \pi \quad (31)$$

and

$$\text{Variance} = \sigma_{\theta_0}^2 = \int_{-\infty}^{\infty} (\theta - \eta_{\theta_0})^2 f_{\theta_0}(\theta) d\theta, \text{ where } |\theta| \leq \pi \quad (32)$$

Substituting Eq.(26) into Eqs.(31) and (32), the mean and variance of the phase can be estimated. For small signal-to-noise ratios, the mean ( $\eta_{\theta_0}$ ) is 0 and the standard

deviation ( $\sigma_{\theta_0}$ ) is  $\pi/\sqrt{3}$  radian.

For large signal-to-noise ratios, the mean phase value is simply  $\theta_0$  and the standard deviation is  $\sigma/a(t_0)$  or  $1/(2 \text{ SNR})^{1/2}$  radian.

## 5.2 Amplitude Error As a Function of Signal-to-Noise Ratio

At time  $t = t_0$ , when the amplitude of the input signal  $a(t) = a(t_0)$ , the probability density function of the envelope is given by[4,6]

$$f_z(z') = z'/\sigma \exp\left[-(z'^2 + 2 \text{ SNR})/2\right] I_0\left[(2 \text{ SNR})^{1/2} z'\right], \text{ for } z' \geq 0 \quad (33)$$

where  $\sigma$  is the standard deviation of the noise in either the I or Q channel and  $z' = z/\sigma$  is the normalized amplitude of the envelope and  $I_0$  is the modified Bessel function of order zero defined by

$$I_0(x) = 1/(2\pi) \int_0^{2\pi} \exp[x \cos(\theta)] d\theta \quad (34)$$

The mean of the envelope is given by

$$E(z') = \eta_{z'} = \int_{-\infty}^{\infty} z' f_z(z') dz', \text{ where } z' \geq 0 \quad (35)$$

and the variance is

$$\sigma_z^2 = \int_{-\infty}^{\infty} (z' - \eta_{z'})^2 f_z(z') dz', \text{ where } z' \geq 0 \quad (36)$$

For small signal-to-noise ratios,

$$f_z(z') \approx z' / \sigma \exp(-z'^2/2), \text{ for } z' \geq 0 \quad (37)$$

which is of Rayleigh distribution and the mean ( $\sigma \eta_{z'}$ ) is  $\sigma(\pi/2)^{1/2}$  and the standard deviation ( $\sigma_z$ ) is  $(2 - \pi/2)^{1/2} \sigma$ .

For large signal-to-noise ratios,

$$I_0[(2 \text{ SNR})^{1/2} z'] \approx \exp[(2 \text{ SNR})^{1/2} z'] / [2\pi (2 \text{ SNR})^{1/2} z']^{1/2} \quad (38)$$

Substituting Eq.(38) into Eq.(33), the probability density function is approximately given by

$$f_z(z') \approx z' / \{\sigma [2\pi (2 \text{ SNR})^{1/2} z']^{1/2}\} \exp\left[-[z' - (2 \text{ SNR})^{1/2}]^2/2\right], \text{ for } z' \geq 0$$

or

$$\approx z' / \left\{ \sigma [2\pi a(t_0)/\sigma z']^{1/2} \right\} \exp\left[-[z' - a(t_0)/\sigma]^2/2\right], \quad (39)$$

for  $z' \geq 0$

Equation (39) is approximately a Gaussian distribution with mean equal to  $a(t_0)/\sigma$ . At  $z' \approx a(t_0)/\sigma$ , the coefficient of the above expression is approximately equal to  $1/[(2\pi)^{1/2}\sigma]$  and thus the standard deviation of the envelope is  $\sigma$ .

## 6.0 MOVING AVERAGE

A moving average is performed on the processed data of the envelope, phase and instantaneous frequency of the signal in the time domain. This is carried out by adding  $N$  contiguous samples and an average is taken on the accumulated sum. The same operation is repeated on the next  $N$  samples. The transfer function is given by[7]

$$H(f)/N = \sin(N\pi f T_s) / [N \sin(\pi f T_s)] \exp[-j(N-1)\pi f T_s] \quad (40)$$

The absolute value of the transfer function is plotted in Fig.7 for various values of  $N$ . As can be seen from the plot, the operation of moving average on the sampled, processed data has the same effect as low-pass filtering in the frequency domain. There are two basic functions performed by using the moving average. The first function is to reduce the video bandwidth and thus the effective noise bandwidth [8] of the I/Q network is reduced with a corresponding improvement on the output SNR. The second function is when there are amplitude and phase imbalances and DC offsets in the I/Q network, there will be ripples introduced on the amplitude, phase and instantaneous frequency as pointed out in Section 3.0. Depending on the frequency of the baseband signal, these ripples can be outside the video bandwidth of the signal of interest and thus reduced by low-pass filtering. The moving average is easy to implement digitally and does not introduce distortions such as ringing and overshoot as other types of filters [9]. As given in Fig. 7, the sidelobe levels are determined by Eq.(40) as a function of  $N$ . For large  $N$ , the first peak sidelobe level is 13.46 dB down and the peak sidelobe level decreases directly proportional to  $1/f$ . If it is desirable to have lower sidelobe levels, a multi-layer moving average can be performed. Fig.8 shows the resultant effect when two layers are used. In this case the data is filtered by a moving average of  $N = 7$  and followed by  $N = 5$ .

## 7.0 EXPERIMENTAL MEASUREMENTS

Implementation of the I/Q network is carried out by the use of a quadrature mixer, a local oscillator and a dual-channel digital scope. The quadrature mixers used are from Anaren Microwave Inc. and KDI/Triangle Electronics Inc. The digital scope is either a 10-bit or 8-bit dual-channel scope from LeCroy Corporation. On any given set of measurements, the set-up is usually "warmed up" for at least 20 minutes before the testing begins. Depending on the type of testing, the actual time taken to complete the test can last over a time period of tens of minutes and sometimes even hours. As a result, if the characteristics of the I/Q network varies as a function of time, they are also reflected in the experimental data.

### 7.1 Imbalance Errors and DC Offsets of I/Q Network

The imbalance errors and DC offsets of I/Q network are measured by using the technique described in Section 4. The I/Q network includes a quadrature mixer, a 3-dB pad, an interconnecting cable and the 10-bit LeCroy 9430 dual-channel digital scope. The 3-dB pad is used to improve the impedance matching between the quadrature mixer and the scope. The in-phase and quadrature signals are sampled and digitized by the scope at a 100-MHz sampling rate with a low-pass filter bandwidth of approximately 150 MHz. Different quadrature mixers are tested as a function of the LO frequency, LO power level and input signal power level. A CW signal from a frequency synthesizer is applied to the input of the I/Q network and is then adjusted to produce a baseband signal from -50 MHz to 50 MHz at 1-MHz steps. A 4000-point DFT is performed on the digitized baseband signals to extract the relative amplitude and phase difference between the two channels and the DC offset in each channel. A typical signal-to-noise ratio of approximately 48 dB is achieved on each sample. When a DFT is performed on 4000 sample points, the signal-to-noise ratio is approximately improved by an additional factor of 36 dB. As a result, the combined signal-to-noise ratio is approximately 84 dB. The noise distribution is approximately Gaussian and the errors introduced by the noise as discussed in Section 5.0 are negligibly small and its effect on the measurements can be neglected.

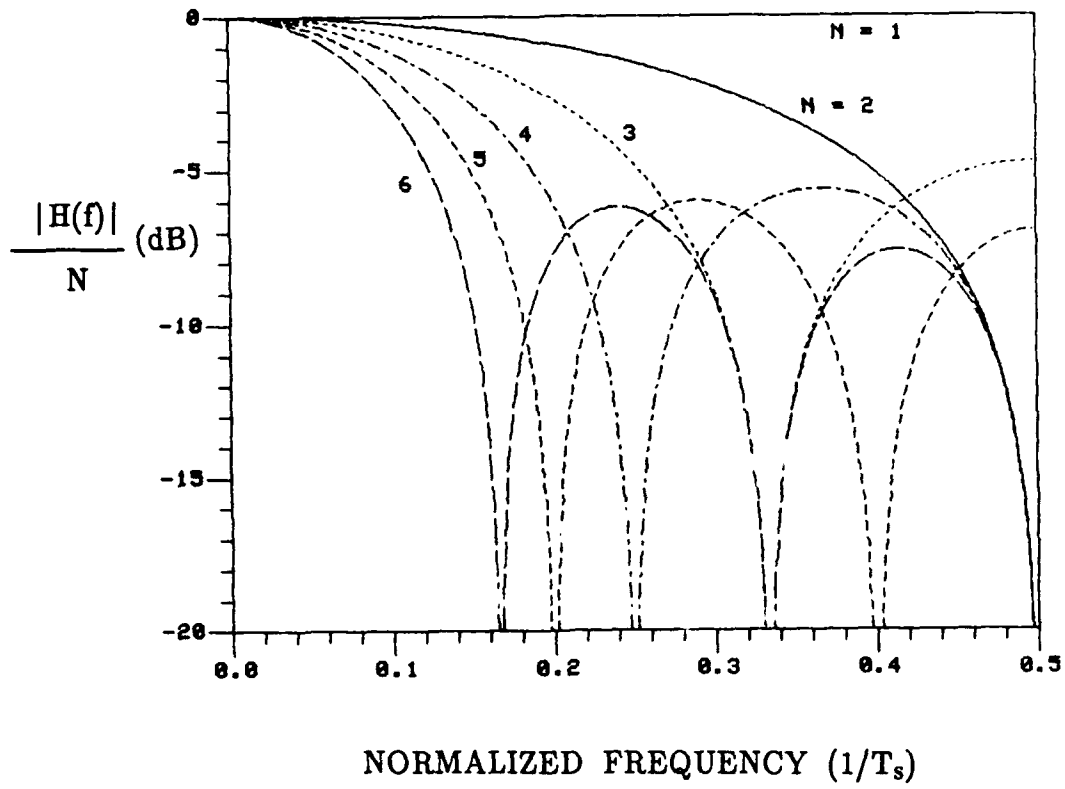


Fig. 7 Transfer Function of Moving Average (Single Layer)

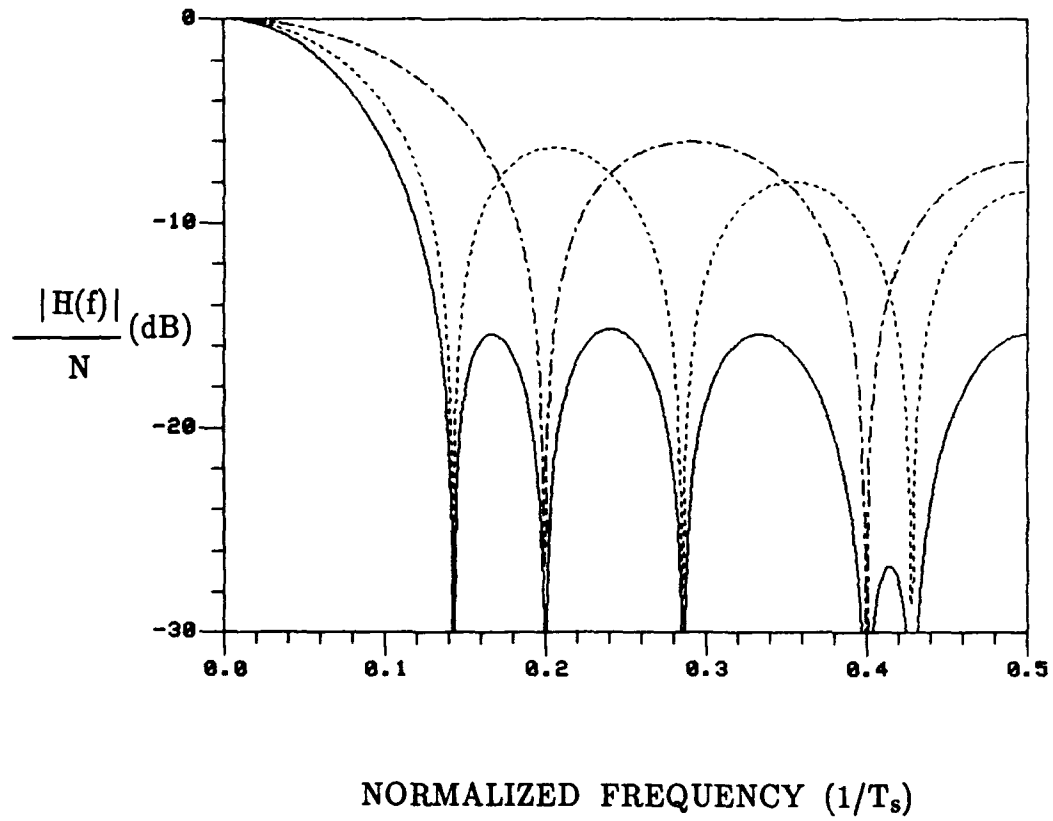


Fig. 8 Transfer Function of Moving Average (Two Layers)

- .....  $N = 7$
- $N = 5$
- $N = 7$  and  $5$

The amplitude ratio  $R$  expressed by  $20 \cdot \log_{10}(K_q/K_i)$  in dB versus baseband frequency is plotted in Fig.9 (a) for a typical I/Q network. The quadrature mixer used is from Anaren Microwave Inc. The LO frequency is set at 1.5 GHz with a power output of 10 dBm. The input signal power level at 1.5 GHz is adjusted so that approximately 80% of full scale deflection is achieved on the digital scope, which is equivalent to  $\pm 32$  mV in a 50- $\Omega$  termination. The same input power level is maintained as the signal frequency is varied. The mean amplitude ratio over the full baseband frequency range of  $\pm 50$  MHz is computed to be 1.034 (0.291 dB). The RMS value is 0.011 and when expressed in terms of  $20 \cdot \log_{10} [( \text{mean} + \text{RMS}) / (\text{mean} - \text{RMS})]$ , it is 0.186 dB.

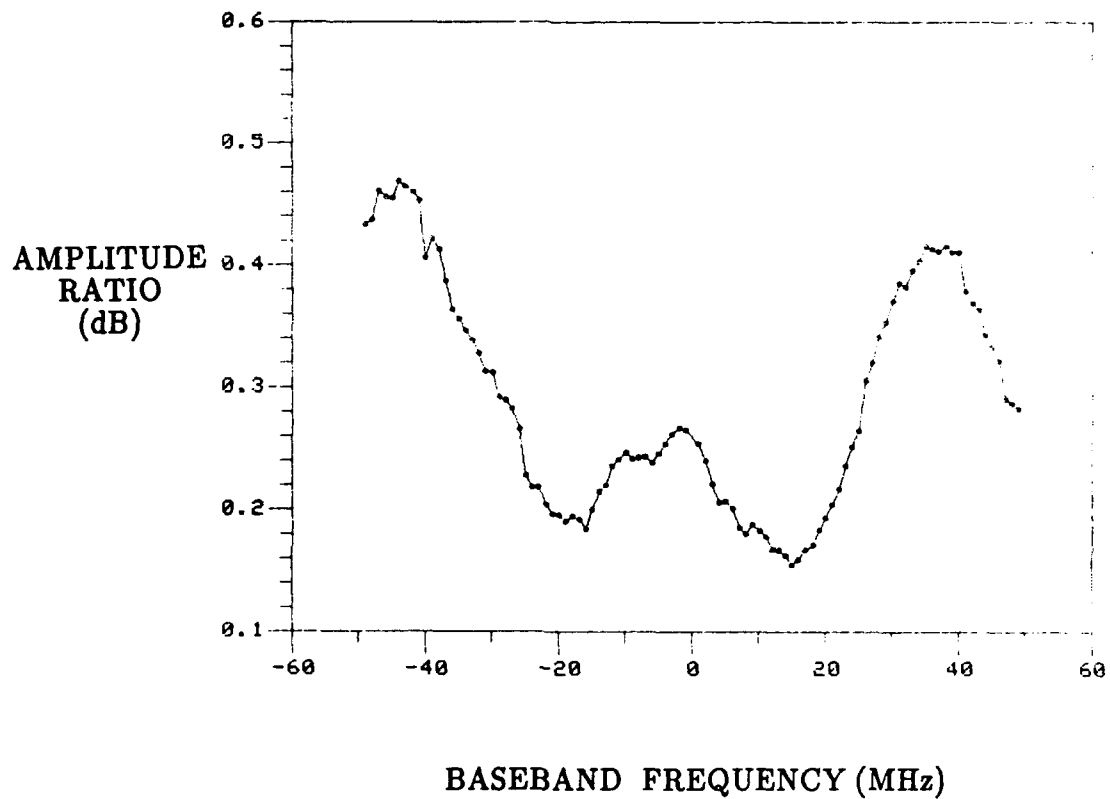
The absolute phase difference between the quadrature channel and the in-phase channel is plotted in Fig.9 (b). The mean value is  $90.46^\circ$  and the RMS value is  $1.81^\circ$ . As can be seen from the plot, the phase difference varies approximately linearly as a function of baseband frequency. As a result, the linear component can be removed by adjusting the cable lengths in both the in-phase and quadrature channels. By applying a least square fit to the data in Fig. 9(b), the absolute phase difference at zero baseband frequency is found to be  $90.465^\circ$ , the slope is  $-0.0606^\circ/\text{MHz}$  and the resultant RMS value is  $0.506^\circ$  over the baseband frequency range of  $\pm 50$  MHz. If the frequency range is reduced to  $\pm 30$  MHz, the absolute phase difference at zero Hz is  $90.365^\circ$ , slope is  $-0.08075^\circ/\text{MHz}$  and the RMS value is reduced to  $0.262^\circ$ .

The DC offsets in mV of both the in-phase and quadrature channels are plotted in Fig.9 (c). The mean DC offset values of the in-phase and quadrature channels are 1.78 mV and  $-2.29$  mV respectively. The RMS values for both the in-phase and quadrature channels are 0.064 mV and 0.073 mV respectively over the baseband frequency range of  $\pm 50$  MHz.

The measured power levels in both the in-phase and quadrature channels are plotted in Fig.9(d) versus baseband frequency.

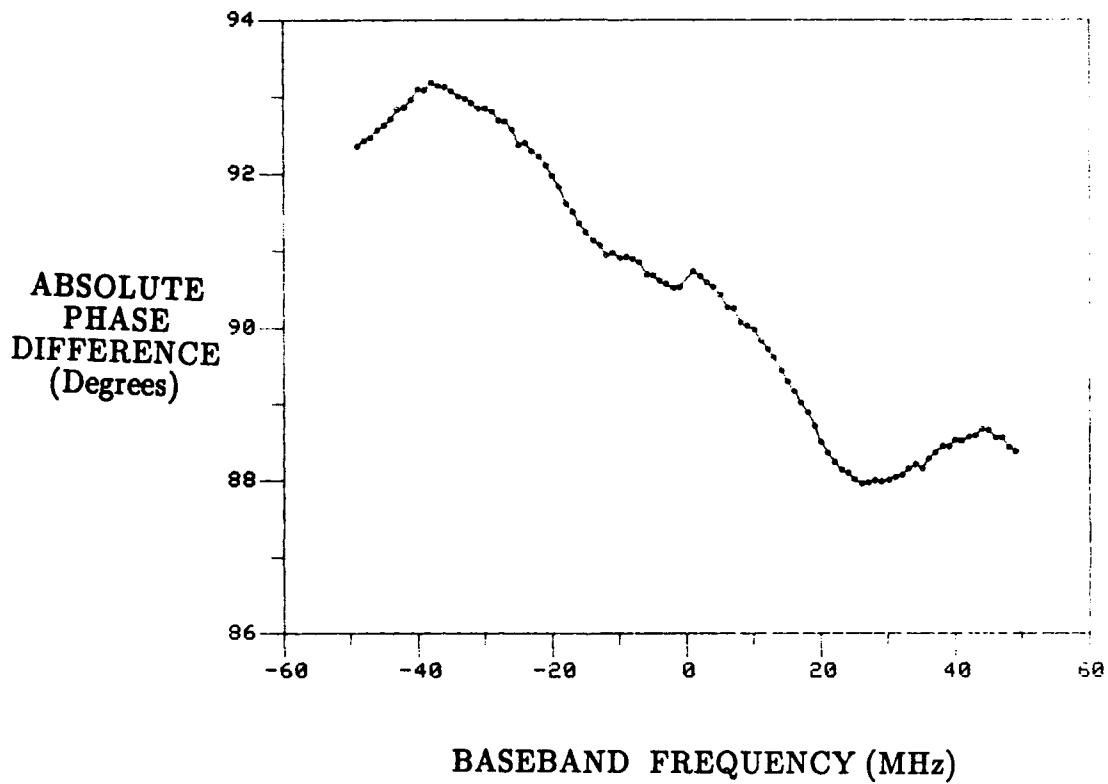
Using the same set-up but with the input signal power reduced by approximately 4 dB as shown in Fig.10 (d), the above set of measurements is repeated. The purpose of this measurement is to evaluate changes in the imbalance errors and DC offsets of the I/Q network as the input signal power level is reduced. The imbalance errors and DC offsets are plotted in Fig. 10(a) to Fig. 10(c). By comparing the two sets of measurements over the full baseband frequency range of  $\pm 50$  MHz, a RMS value on the difference in amplitude ratio is found to be 0.00318, a phase difference of  $0.126^\circ$  and DC offsets of 0.137 mV and 0.223 mV in the in-phase and quadrature channels respectively. As a result, there are negligible differences in the imbalance errors and DC offsets when the input power level is reduced by 4 dB.

Another set of measurements is taken to evaluate the imbalance errors and DC offsets over a much wider input signal power range for one specific signal frequency. The signal frequency is set at 1040 MHz while the LO frequency is at 1 GHz with a power output of approximately 13 dBm. The input signal power level is varied in 3-dB steps and at each step, the imbalance errors and DC offsets of the I/Q network are computed. They are plotted in Fig. 11(a) to Fig. 11(c). As the input power is reduced, the output signal-to-noise ratio is also reduced. In order to compensate for the reduced output



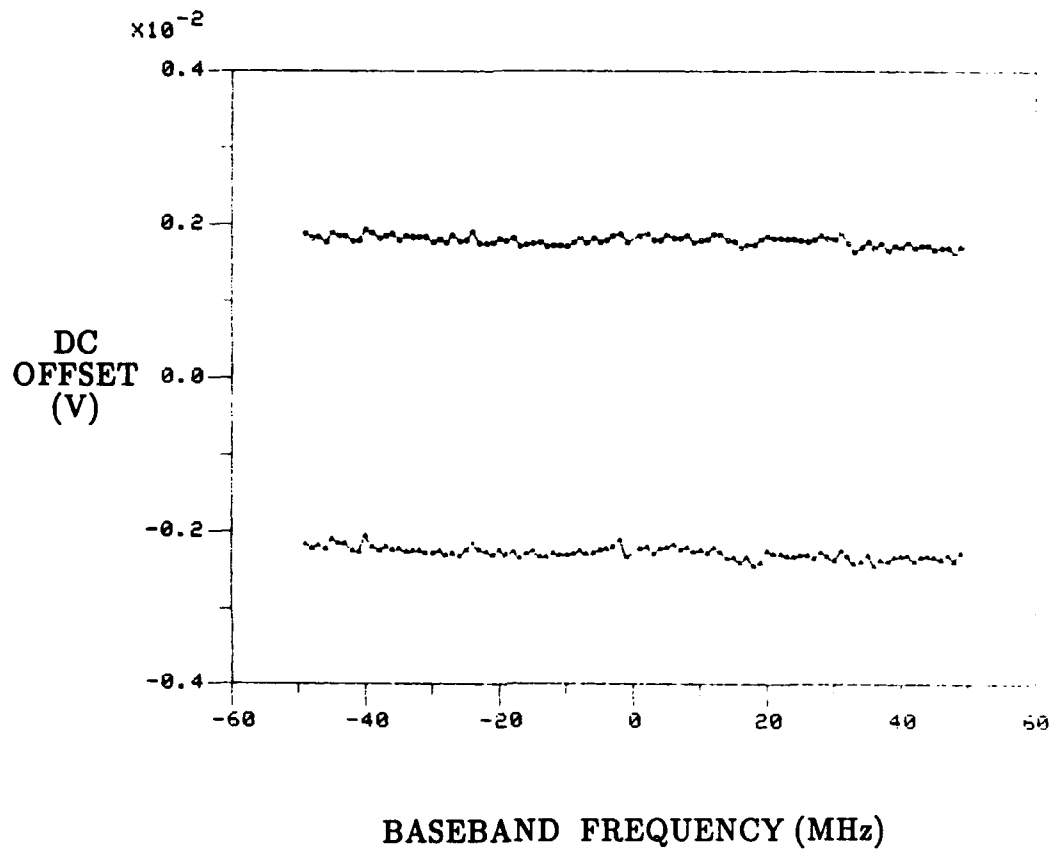
(a) Amplitude Ratio Versus Baseband Frequency

Fig.9 Imbalance Errors and DC Offsets of I/Q Network  
 ( Input Signal Power Level  $\approx -19$  dBm)



(b) Absolute Phase Difference Versus Baseband Frequency

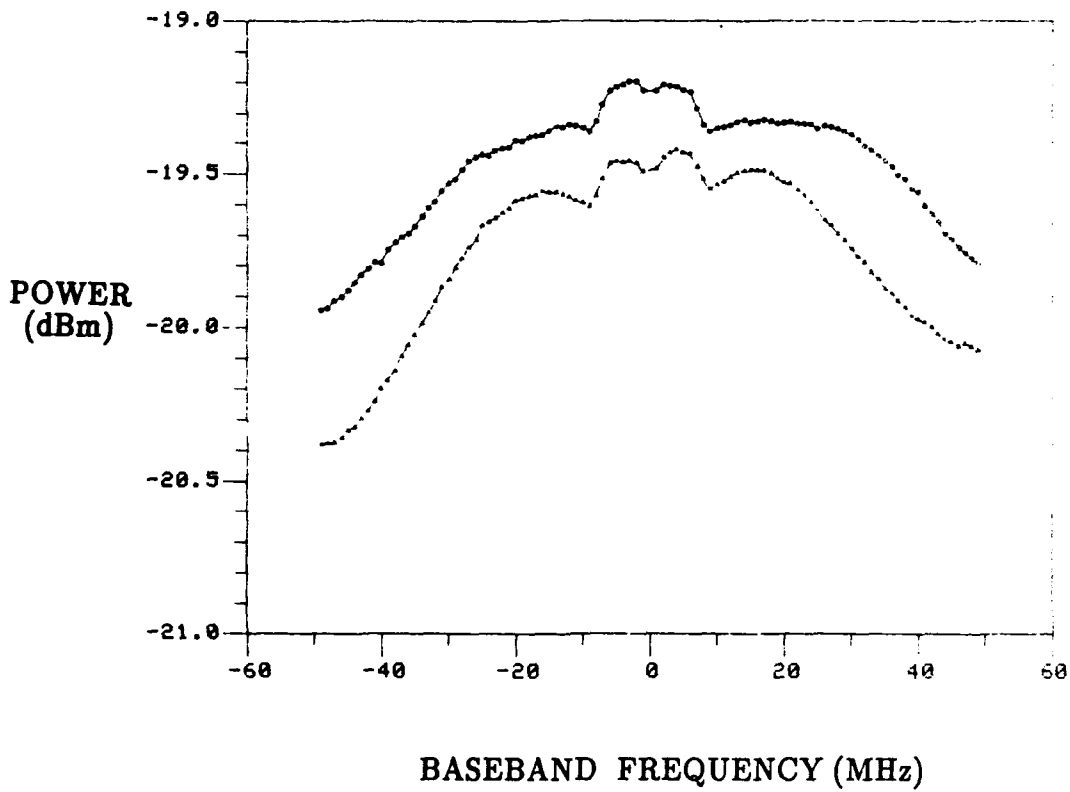
Fig.9 Imbalance Errors and DC Offsets of I/Q Network  
( Input Signal Power Level  $\approx -19$  dBm)



(c) DC Offsets Versus Baseband Frequency

—○—○—○— In-phase Channel  
 —▲—▲—▲— Quadrature Channel

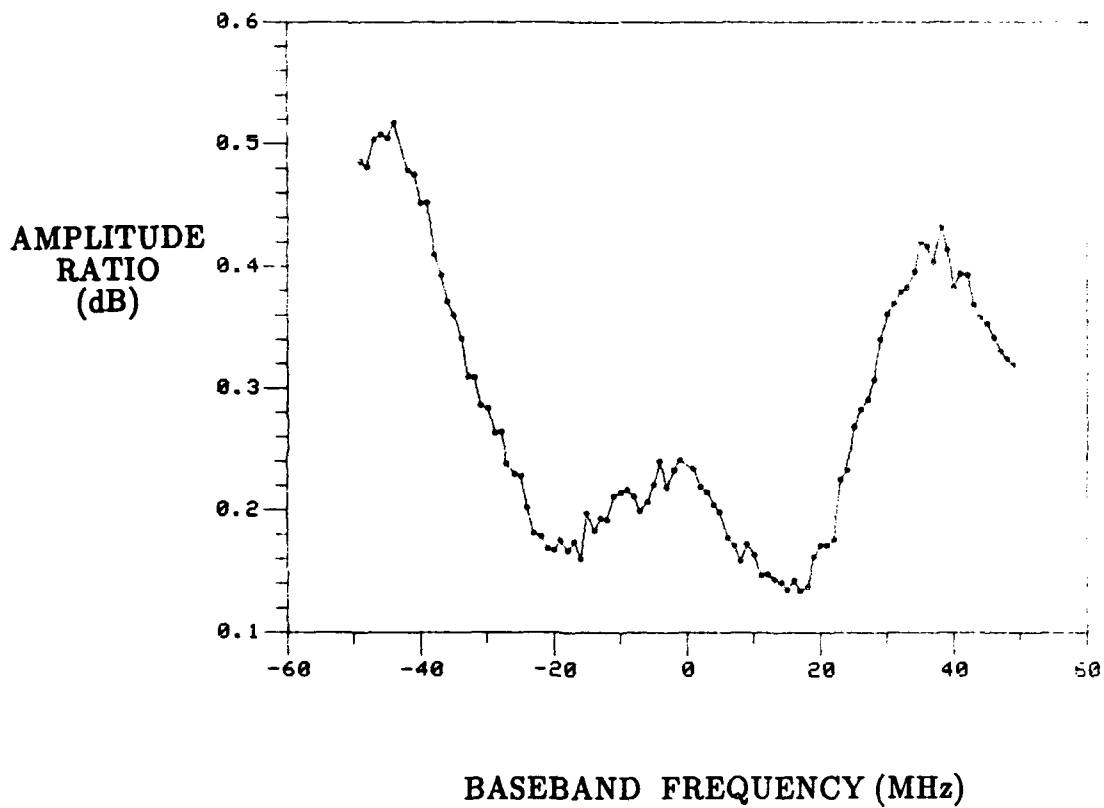
Fig.9 Imbalance Errors and DC Offsets of I/Q Network  
 ( Input Signal Power Level  $\approx -19$  dBm)



(d) Power Output Levels Versus Baseband Frequency

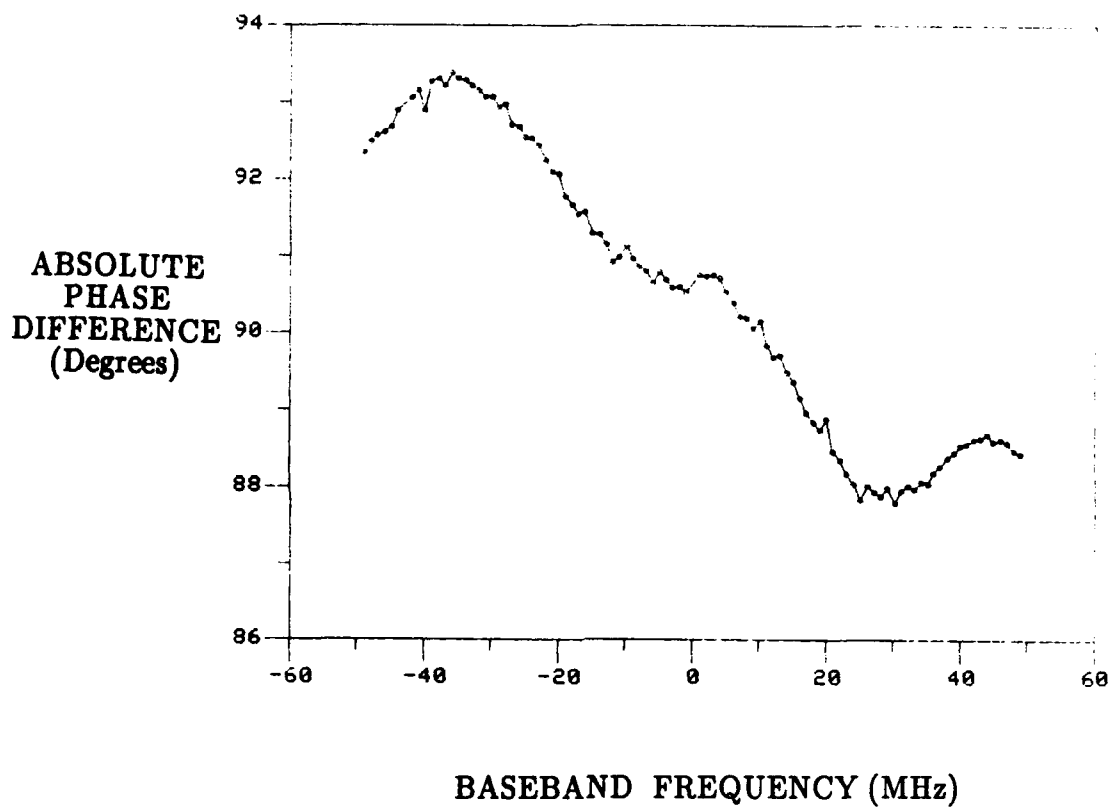
—○—○—○— In-phase Channel  
 —▲—▲—▲— Quadrature Channel

Fig.9 Imbalance Errors and DC Offsets of I/Q Network  
 ( Input Signal Power Level  $\approx -19$  dBm)



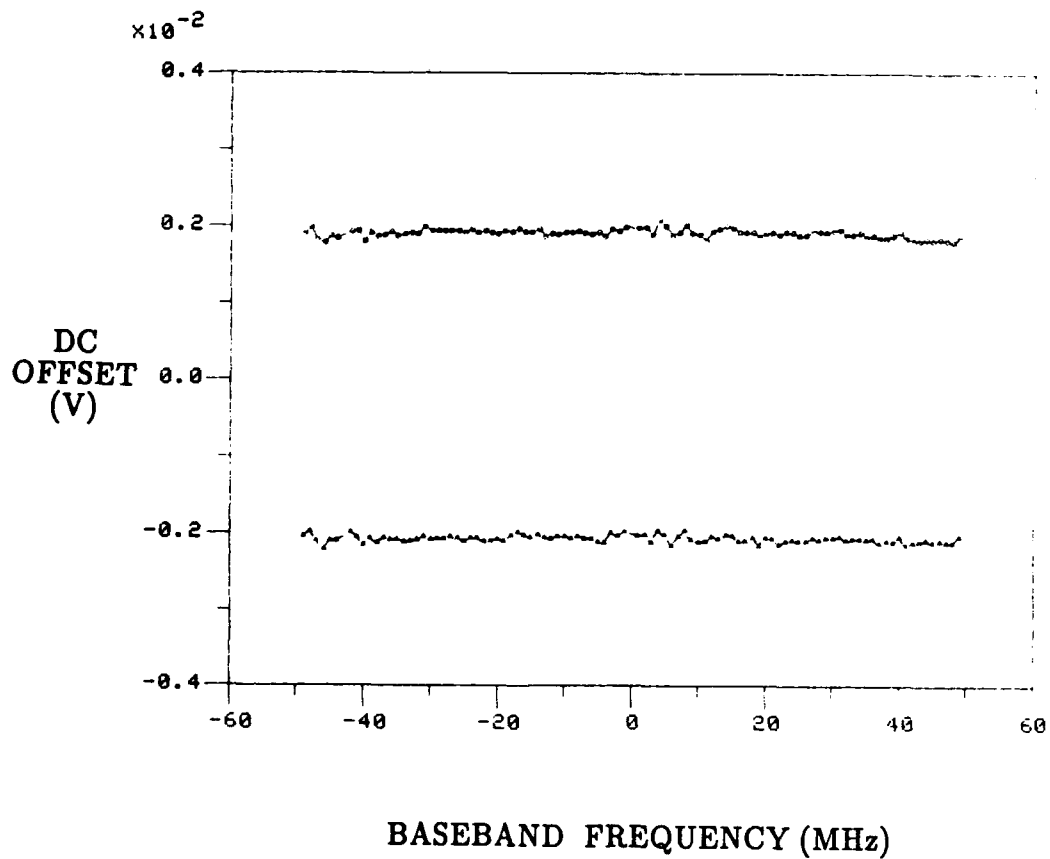
(a) Amplitude Ratio Versus Baseband Frequency

Fig.10 Imbalance Errors and DC Offsets of I/Q Network  
 ( Input Signal Power Level  $\approx -23$  dBm)



(b) Absolute Phase Difference Versus Baseband Frequency

Fig.10 Imbalance Errors and DC Offsets of I/Q Network  
( Input Signal Power Level  $\approx -23$  dBm)

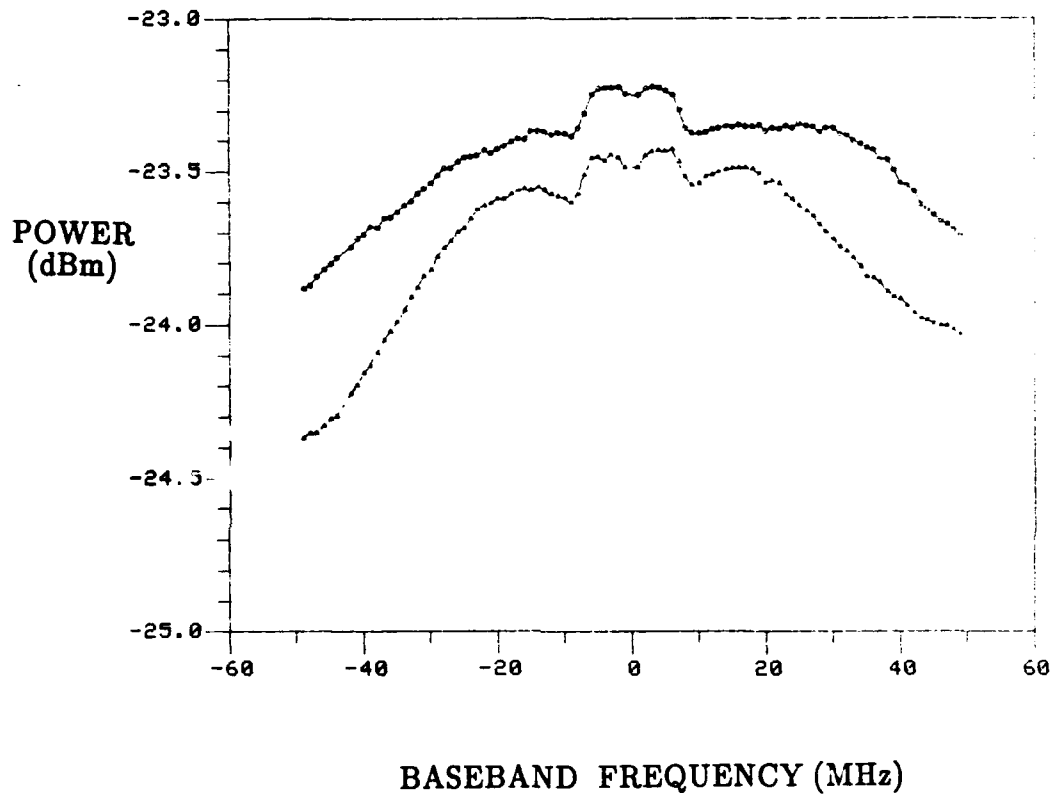


(c) DC Offsets Versus Baseband Frequency

—○—○—○— In-phase Channel

—▲—▲—▲— Quadrature Channel

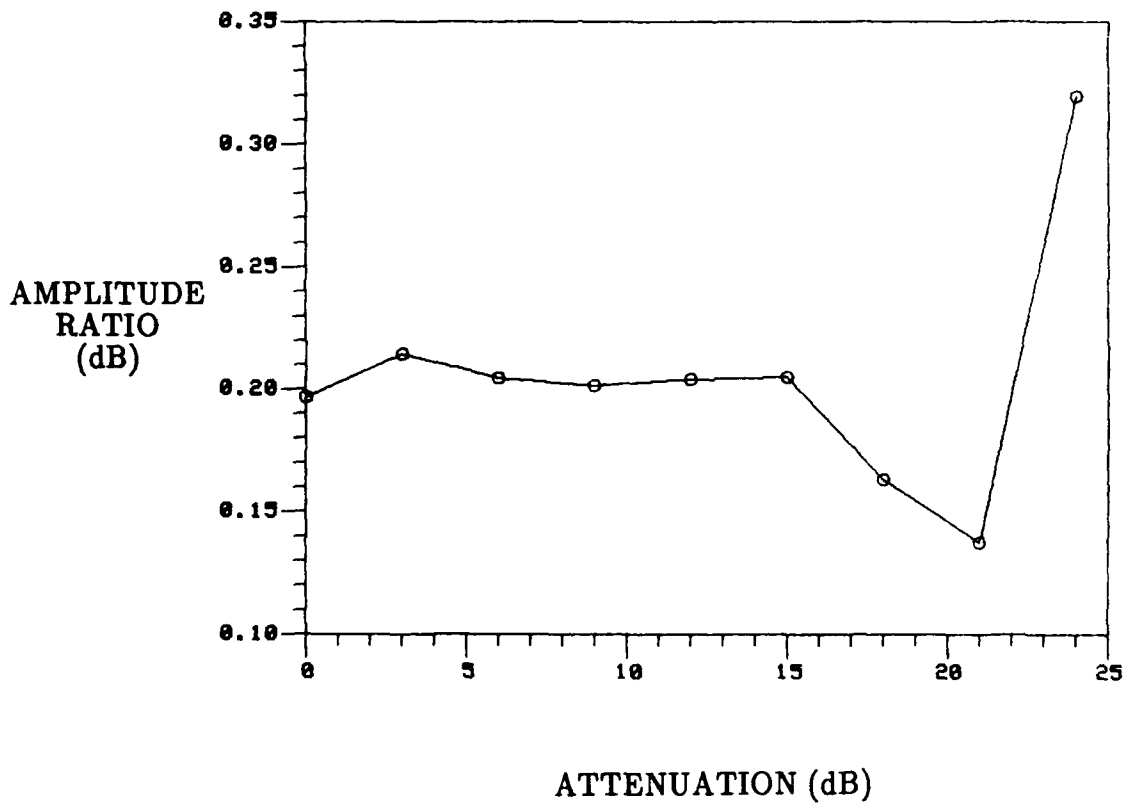
Fig.10 Imbalance Errors and DC Offsets of I/Q Network  
( Input Signal Power Level  $\approx -23$  dBm)



(d) Power Output Levels Versus Baseband Frequency

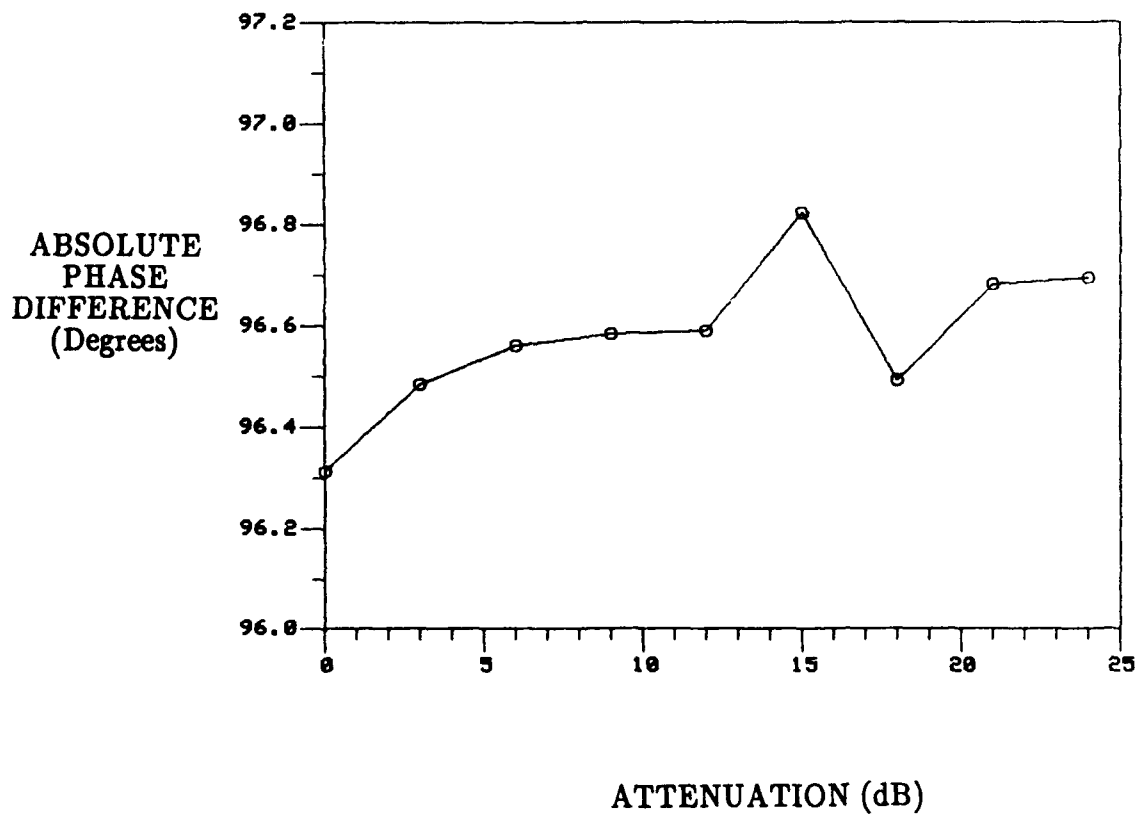
—○—○—○— In-phase Channel  
 —▲—▲—▲— Quadrature Channel

Fig.10 Imbalance Errors and DC Offsets of I/Q Network  
 ( Input Signal Power Level  $\approx -23$  dBm)



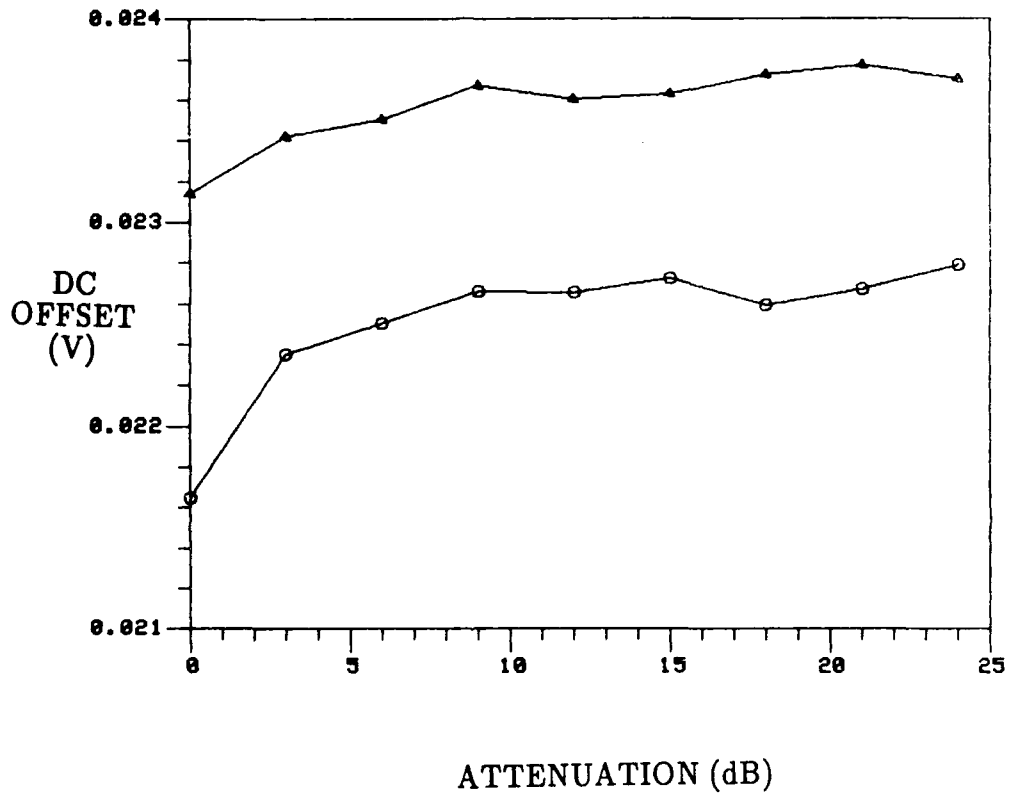
(a) Amplitude Ratio Versus Input Signal Level

Fig. 11 Imbalance Errors and DC Offsets of I/Q Network Versus Input Signal Level



(b) Absolute Phase Difference Versus Input Signal Level

Fig. 11 Imbalance Errors and DC Offsets of I/Q Network Versus Input Signal Level



(c) DC Offsets Versus Baseband Input Signal Level

—○—○—○— In-phase Channel

—▲—▲—▲— Quadrature Channel

Fig. 11 Imbalance Errors and DC Offsets of I/Q Network Versus Input Signal Level

signal-to-noise ratio, more sample points are needed for the DFT. For this set of measurements, the number of sample points has been increased from 4,000 to 40,000. As can be seen from the graphs, the imbalance errors and DC offsets do vary slightly over the 24-dB testing range.

Under different operating conditions, the imbalance errors and DC offsets of the I/Q network have also been evaluated. It is found that the imbalance errors and DC offsets are a strong function of the LO frequency and power level to the quadrature mixer. Once the optimum operating LO frequency and power level are chosen and fixed, the imbalance errors and DC offsets are relatively insensitive to input signal power level and frequency.

In summary, the mean imbalance errors and DC offsets of typical I/Q networks over a large frequency range can be large. In order to keep the systematic errors small, some form of calibration is needed to remove the means of the imbalance errors and DC offsets. Once the means are removed, the RMS values of the imbalance errors and DC offsets as a function of signal frequency and power is quite small. If further reduction in the systematic errors is required, a more elaborate calibration is required as a function of the signal frequency and may even the signal power.

## 7.2 Amplitude, Phase and Instantaneous Frequency Measurement Versus Input SNR

For this set of measurements, a CW signal from a frequency synthesizer is amplified by two high gain IF amplifiers before it is applied to the I/Q network. The total noise appearing on the scope is dominated by the noise from the first amplifier and is of Gaussian distribution with zero mean. The signal and noise in the in-phase and quadrature channels are sampled and digitized at a rate of 100 MHz. The frequency of the CW signal from the synthesizer is finely tuned so that the resultant baseband signal is almost completely phase-locked to the clock of the digital scope. This is carried out to make the number of sampled phases of the input signal to be the smallest. Once the number of discrete phases of the samples are determined, the samples can then be sorted out easily into groups of identical input phases. For example, if the LO and input signal are set at 1 GHz and 1020 MHz respectively, the resultant baseband signals are at 20 MHz. When the baseband signals are phase-locked to the sampling scope at 100 MHz, for every cycle of the input signal, exactly five samples are generated with a phase difference of 72 degrees. These same five input phases of the input signal are sampled repeatedly for subsequent cycles to produce five identical groups of samples. In the measurement, the phase of the input signal is kept phase-locked to the sampling scope to better than 0.036 degrees over a total number of 5,000 samples. The in-phase and quadrature signals are first compensated to remove the imbalance errors and DC offsets by using the procedure as outlined in Section 4.0. A total of 5,000 samples, with five groups of 1,000 samples each, are then used to compute the means and RMS values of the envelope and phases of the input signal. A large signal is first applied to the scope to obtain approximately 90% total deflection. At this high SNR, the output amplitude of the envelope is approximately of Gaussian distribution as given by Eq.(39). When the number of samples is large, the ratio of the measured RMS value to the mean is approximately equal to  $\sigma/a$  and thus the input SNR is approximately given by  $[a^2/(2\sigma^2)]$ . Next, the input signal is attenuated by 3 dB and the means and RMS values of the envelope and phases are then computed again.

Using the above set-up and measurement procedures, the statistics on the measured envelope and phases are generated at a baseband frequency of 20 MHz and 40 MHz.

As expected, the statistics are found to be independent of frequency.

The RMS phase error in degrees as a function of input SNR in dB is plotted in Fig.12 for the case when the baseband frequency is at 40 MHz. The circles are the experimental points while the solid curve is obtained by using Eqs.(26), (31) and (32). As can be seen from Fig. 12, the experimental measurement agrees very well with theory. For small input SNR, the RMS phase error is quite large. As the input SNR is increased, the RMS phase error decreases rapidly, and for large input SNR, the RMS value decreases inversely proportional to the square root of the input SNR.

The ratio of the RMS value to the mean of the envelope in dB, at a baseband frequency of 40 MHz, versus input SNR in dB is plotted in Fig.13. The theoretical curve is calculated by using Eqs.(33) ,(35) and (36). As expected, the experimental measurement agrees very well with the theory. As discussed in Section 5.2 , the probability density function is a Rayleigh distribution for small SNR. As a result, the ratio of the standard deviation to the mean is a constant and equals to  $[(4 - \pi)/\pi]^{1/2}$  or  $-5.63$  dB. For large input SNR, the ratio of the standard deviation to the mean in dB is inversely proportional to input SNR in dB.

Once the samples on the phase of the signal are generated, its approximate instantaneous frequency can also be determined by using the relationship given by Eq.(7). An experiment is carried out to evaluate the instantaneous frequency error as a function of input SNR and baseband frequency. A band-pass filter centered at 750 MHz with a 3-dB bandwidth of 40 MHz is inserted between the two IF amplifiers and the I/Q network. The same procedure as described above is used to compute the phase values of the input signal as the input SNR is varied. The LO frequency is set at 750 MHz with an output power of 10 dBm. Three different IF frequencies of 755 MHz, 760 MHz and 770 MHz are used to generate baseband frequencies corresponding to 5 MHz, 10 MHz and 20 MHz respectively. For instance, when the frequency of the baseband signal is at 20 MHz, five groups of identical input phase samples of 1000 each are generated. The RMS value on the difference in phase between consecutive samples are calculated and then normalized by the RMS phase error of the samples. The normalized RMS phase difference as a function of input SNR is plotted in Fig. 14 for the three different baseband frequencies. The cross-covariance between consecutive samples is also computed and then normalized by the RMS phase error of all the samples. The normalized cross-covariance as a function of input SNR is plotted in Fig. 15. By comparing the two plots, there is a close correspondence between the two. In other words, when the cross-covariance is small, the phase error from sample to sample is less correlated and thus a higher RMS phase difference.

A simulation has also been carried out to verify the results in Figs. 14 and 15. White Gaussian random noise with zero mean is first filtered by a Butterworth low-pass filter of 20-MHz bandwidth before it is added to the baseband signals. The Butterworth filter is of 1st order having less than 3 dB of attenuation at 20 MHz and 15 dB down by 30 MHz. The in-phase and quadrature noises are uncorrelated. The baseband frequencies used are DC, 5 MHz, 10 MHz and 20 MHz. The RMS value on the difference in phase between consecutive samples is calculated and then normalized by the RMS phase error of the samples. The normalized RMS phase difference as a function of input SNR is plotted in Fig. 16.

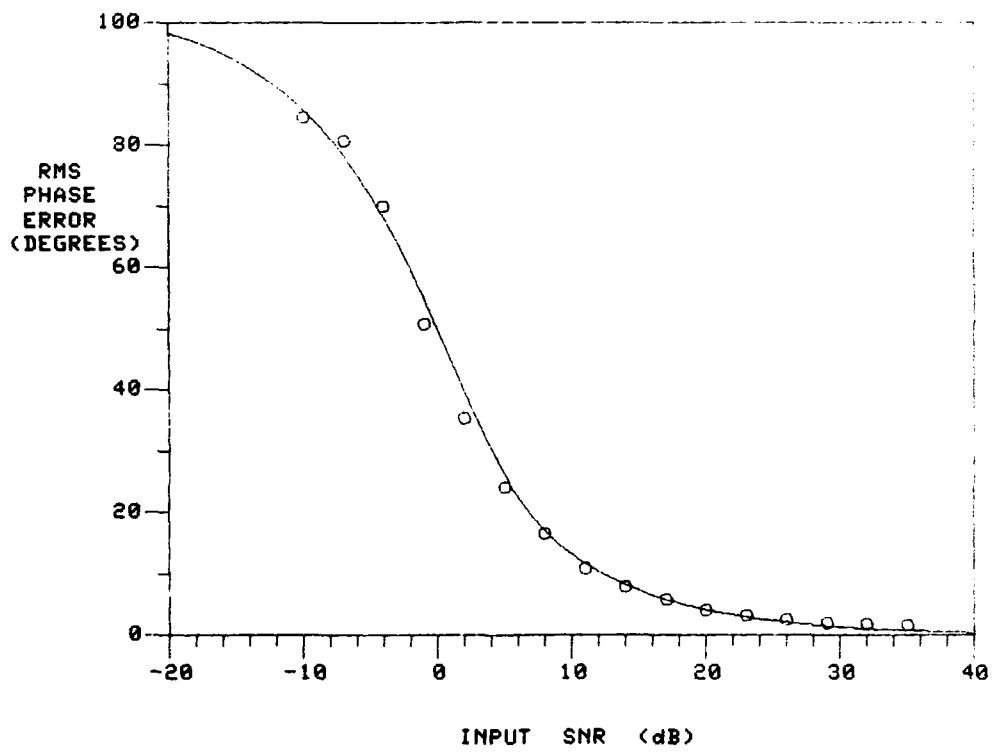


Fig. 12 RMS Phase Error Versus Input SNR

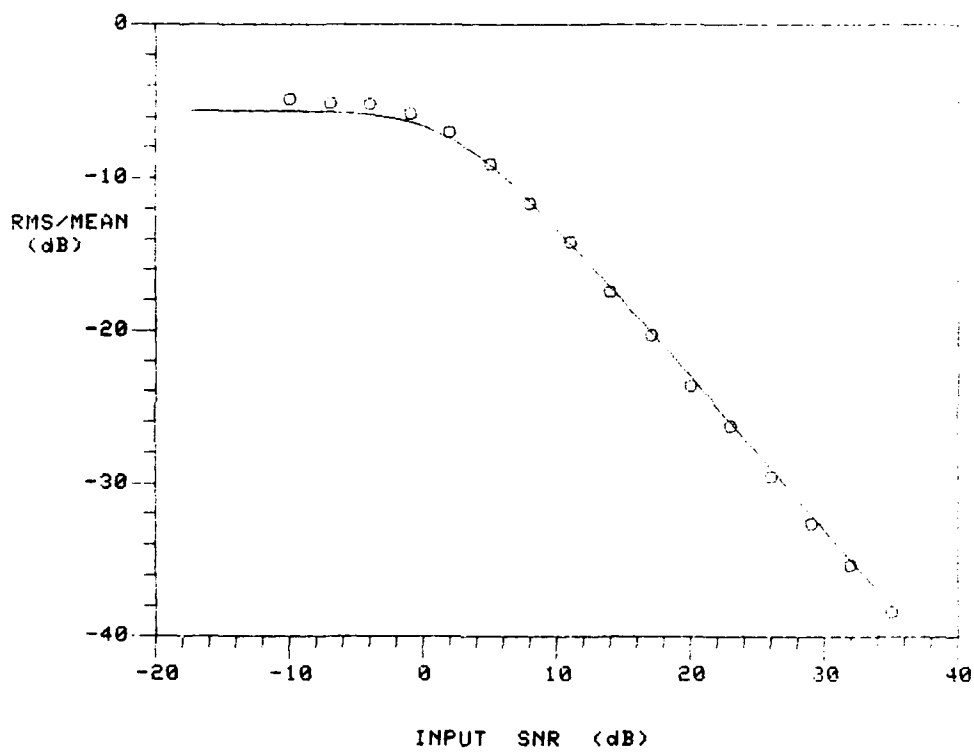


Fig. 13 Ratio of RMS Amplitude Error to Mean Versus Input SNR

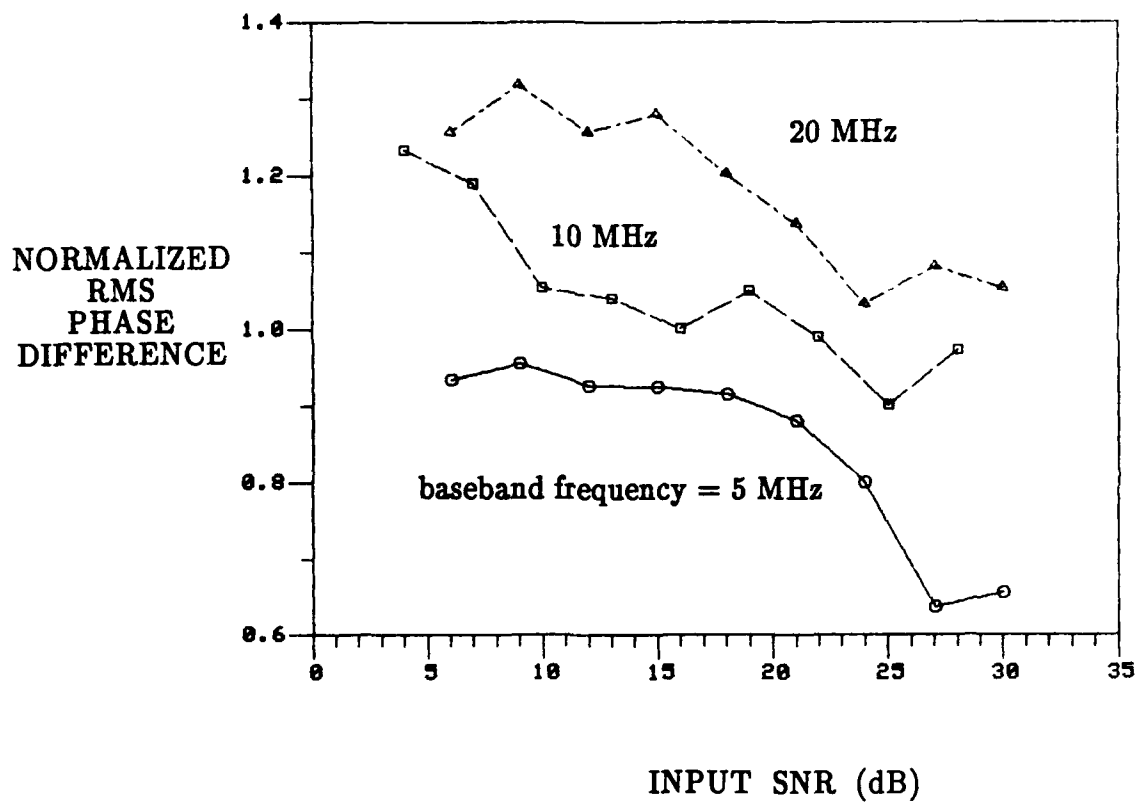


Fig. 14 Normalized RMS Phase Difference Versus Input SNR  
Using Experimental Data ( Noise Bandwidth = 20 MHz )

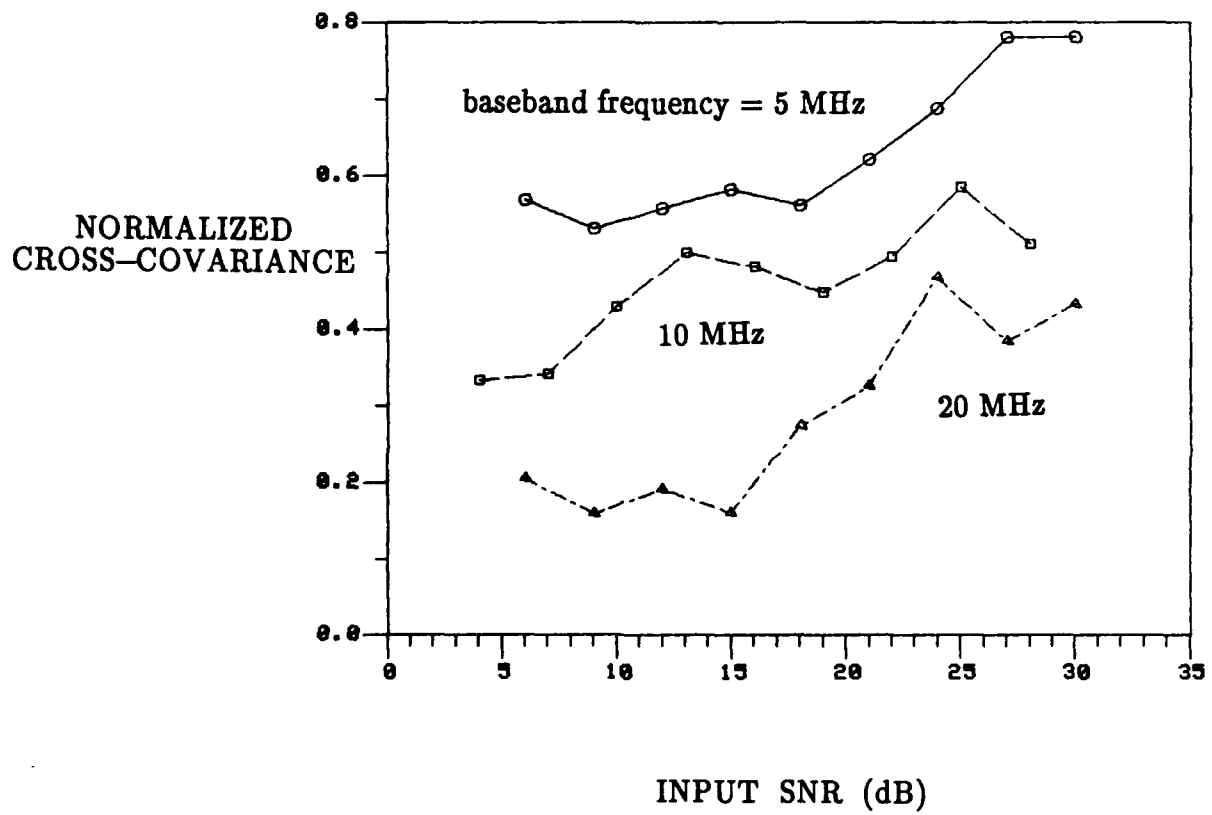


Fig. 15 Normalized Cross-Covariance Versus Input SNR  
Using Experimental Data ( Noise Bandwidth = 20 MHz )

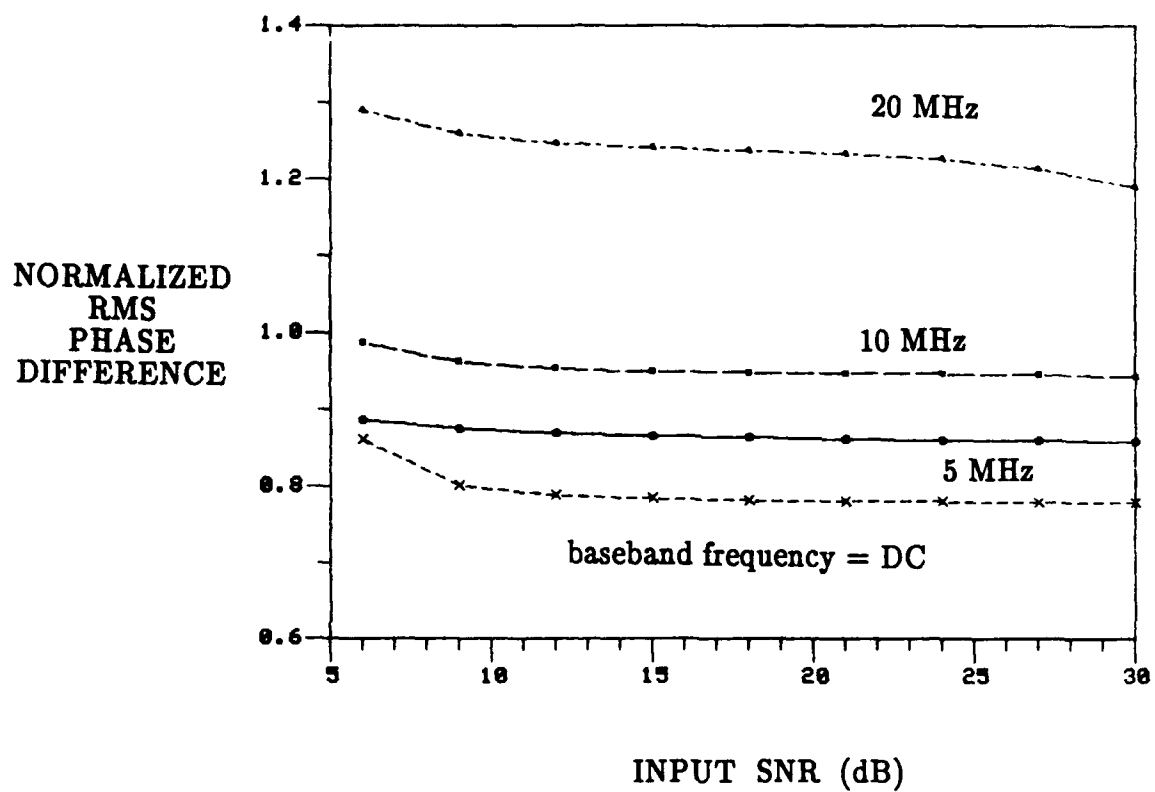


Fig. 16 Normalized RMS Phase Difference Versus Input SNR  
Using Simulated Data ( Noise Bandwidth = 20 MHz )

At large input SNR, the phase error due to noise before it is applied to the I/Q network can be approximated by [10]

$$\Delta\theta_o(t) = \tan^{-1}\left[n_s(t)/[a(t)+n_c(t)]\right] \approx n_s(t)/a(t) \quad (41)$$

where the input noise is represented by its narrow-band quadrature components  $n_c(t)$  and  $n_s(t)$ . Both  $n_c(t)$  and  $n_s(t)$  are of Gaussian distribution with zero mean and of equal variance. Furthermore, they are uncorrelated. Both  $n_c(t)$  and  $n_s(t)$  have a spectral density of  $\eta$  over the frequency range of  $|f| \leq B_{IF}/2$ . As discussed in Section 5.0, after both the noise and signal are mixed down to baseband, the phase error is still approximately given by Eq.(41). The standard deviation of the phase error is given by

$$\sigma_{\theta_o} = \sigma/a(t_o) = 1/(2 \text{ SNR})^{1/2} \quad (42)$$

$\sigma_{\theta_o}$  is found to be independent of the baseband frequency of the signal. When the baseband frequency of the CW signal is taken into account to obtain the absolute phase, a linear phase progression is introduced as

$$\theta(t) = \theta_o(t) + \Delta\theta_o(t) \approx \beta(t) + n_s(t)/a(t) \quad (43)$$

where  $\beta(t)$  is the phase function of the baseband signal and is directly proportional to the baseband frequency. When the baseband frequency is not DC, the spectral density of  $n_s(t)$  is shifted by the baseband frequency. As a result, the spectral density of the noise which is centered at DC has been shifted to a higher frequency by the baseband frequency of the signal. When the spectral density of the noise is shifted, the cross-correlation between consecutive phase samples is affected. In the case where the baseband frequency is comparable to the noise bandwidth and is much less than the sampling frequency, a shift in the noise spectral density by the baseband frequency is expected to have a greater impact on the cross-correlation of the phase samples. The phase error from sample to sample is expected to be less correlated, thus giving a higher normalized RMS phase difference.

The normalized cross-covariance is also computed and plotted in Fig. 17. As expected, there is a close correspondence between the RMS phase difference and its cross-covariance.

By comparing the experimental measurement to the result of the simulation, there is a general agreement between the two. The experimental results are less accurate at high input SNR where the phase errors due to noise are very small and the phase noise from the synthesizers is significant. Another source of error is that the signal source and local oscillator are not truly phase-locked with the clock of the sampling scope.

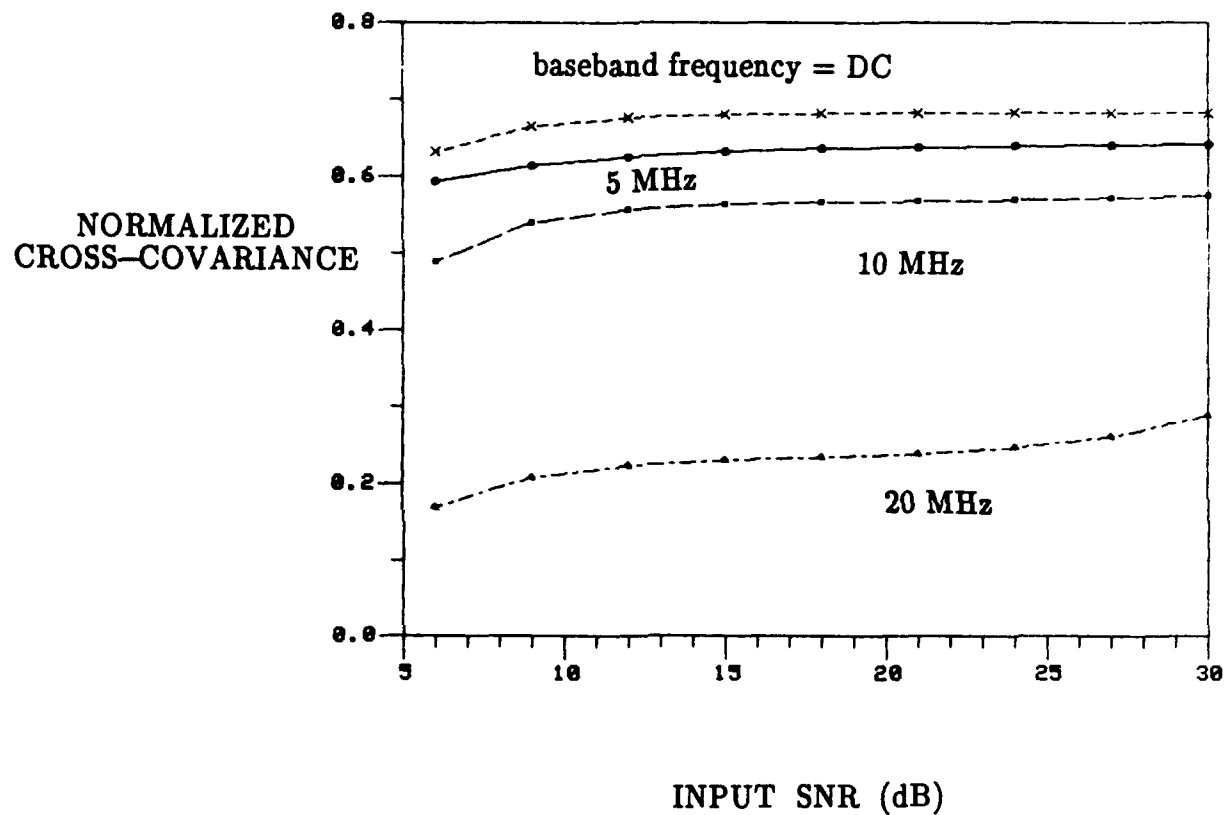


Fig. 17 Normalized Cross-Covariance Versus Input SNR  
Using Simulated Data ( Noise Bandwidth = 20 MHz )

Another simulation has carried out by increasing the bandwidth of the Butterworth low-pass filter to 40 MHz. The Butterworth filter is of 3rd order having less than 3 dB of attenuation at 40 MHz and 15 dB down by 45 MHz. The sampling rate is still 100 MHz. The normalized RMS phase difference as a function of input SNR is plotted in Fig. 18. In this case, the noise spectral density is almost uniform across the full frequency band, and the consecutive phase error is expected to be much less correlated as shown. As the baseband frequency of the signal is slightly increased, the spectral density of the noise will be shifted up and aliasing will become more severe. The exact cross-correlation will be more complicated to analyze. The normalized cross-covariance is also computed and plotted in Fig. 19.

Once the phase errors between consecutive samples are known, the instantaneous frequency error can then be computed directly. when the phase error from sample to sample is uncorrelated, the normalized RMS phase difference is expected to be equal to  $(2)^{1/2}$ . In most practical cases, this would represent the upper limit on the error.

### 7.3 I/Q Demodulation of Signals

In this section, two examples are used to illustrate the effectiveness of calibration and moving averages on the demodulation of radar signals. Implementation of the I/Q network is carried out by the use of a quadrature IF mixer from Anaren Inc.. The LO frequency is set at 2 GHz with an output power of 10 dBm. The in-phase and quadrature signals are digitized using the LeCroy 9450 dual-channel 8-bit digital scope. The radar signals are generated using the HP 8791 Frequency Agile Signal Simulator. The process of compensation and computation is carried out in software.

#### 7.3.1 Pulse Modulated CW Signal

A pulse modulated CW signal at 1960 MHz with a pulse width of approximately 0.5  $\mu$ s is applied to the I/Q network. Figures 20 and 21 show the measured envelope and instantaneous frequency respectively of the pulse modulated CW signal. The raw data of the envelope is plotted in Fig.20(a) for an input SNR of approximately 28 dB. The imbalance errors and DC offsets at this frequency are measured to be as follows:  $R = 0.847$ ,  $(\phi_q - \phi_i) = 2.92$  degrees,  $a_{q0}/[aK_q/2] = -0.55\%$  and  $a_{i0}/[aK_i/2] = 5.1\%$ . The DC offsets are very small as compared to the phase and amplitude imbalances. As discussed in Section 3.1, the computed ripples are expected to have a dominant frequency of 80 MHz, which is twice that of the baseband frequency (40 MHz). However, since the computed output is sampled (plotted) at an interval of 10 ns per sample which corresponds to a sampling rate of 100 MHz, there will be aliasing effects introduced. As a result, the aliased frequency of the ripples is now at 20 MHz (100-80) as shown. Figure 20(b) shows the effect of applying a 7-point moving average. As expected the low-pass filtering has the effect of reducing the amplitude of the ripples and at the same time has also rounded off the pulse edges slightly. A more logical approach is to use the compensation technique first to minimize the errors caused by the imbalance errors and DC offsets and then use a moving average, as shown in Fig. 20(c). The mean of the envelope is measured to be -13.1 dBm while the RMS value is -32.56 dBm. The measured peak-to-peak RMS value  $\{20 \cdot \log_{10} [(mean + RMS)/(mean - RMS)]\}$  is 0.098 dB. The ratio of the mean to the RMS value is higher than the input SNR because not all of the systematic errors have been removed. When a moving average is

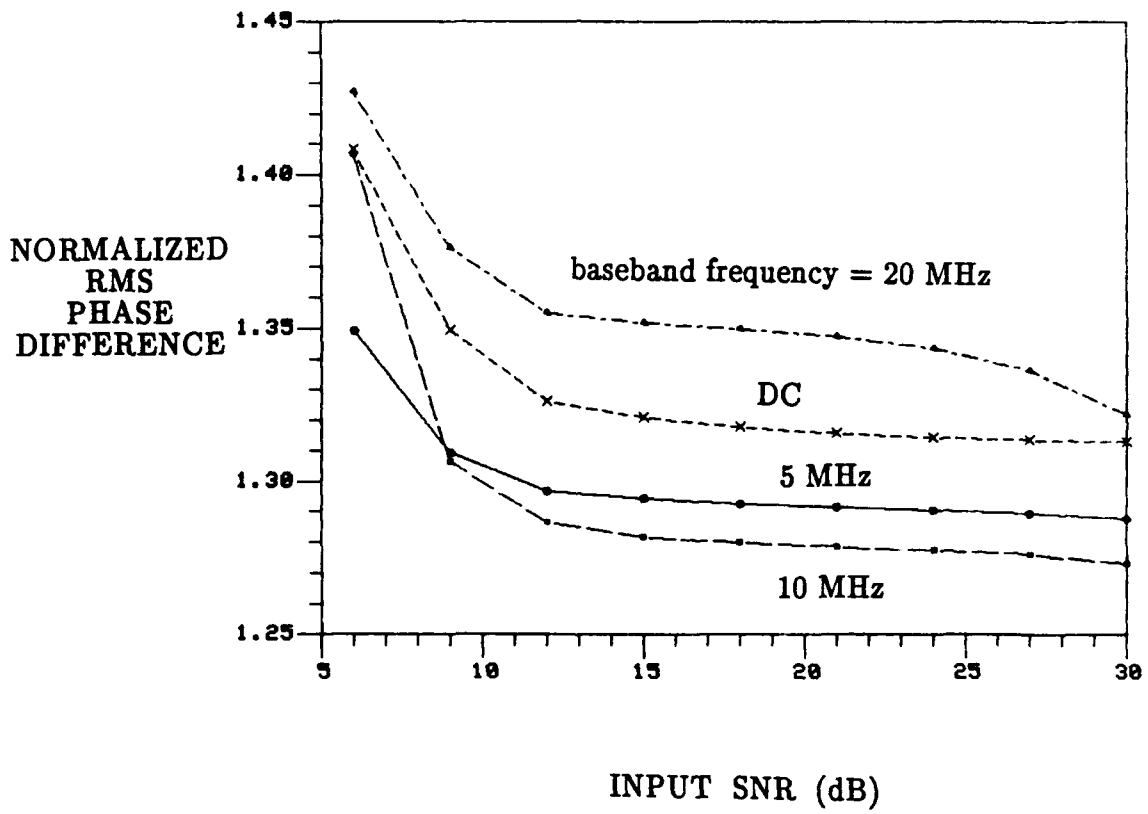


Fig. 18 Normalized RMS Phase Difference Versus Input SNR  
Using Simulated Data ( Noise Bandwidth = 40 MHz )

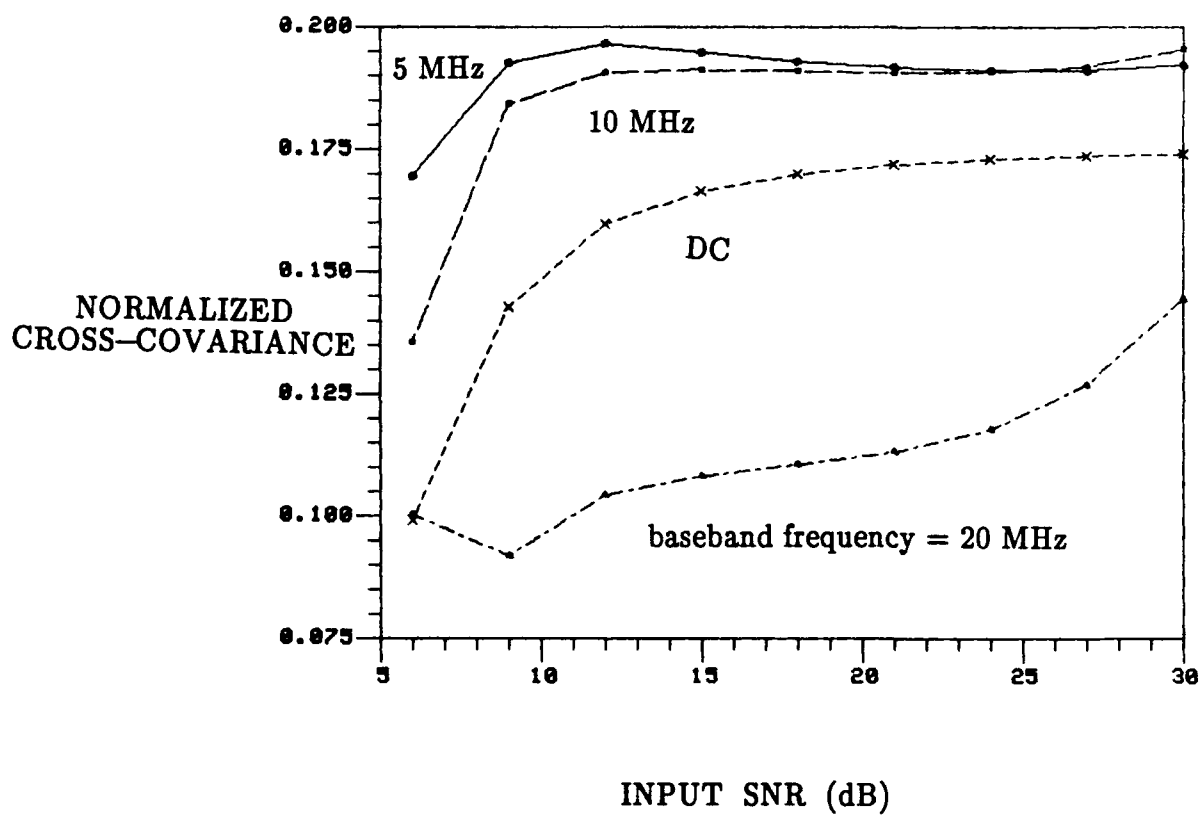
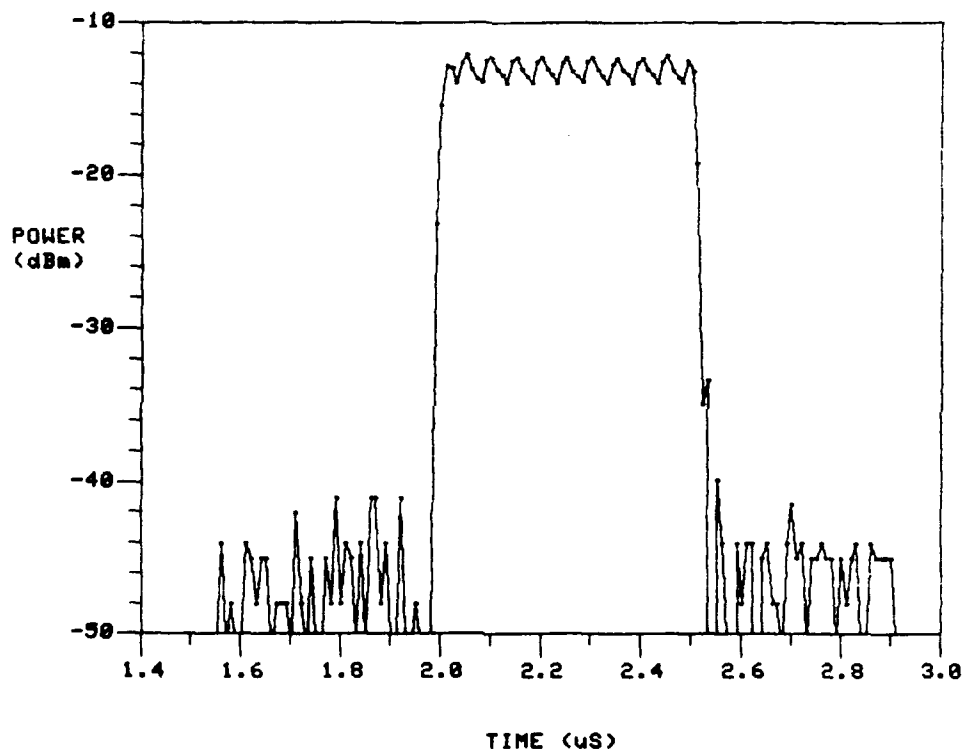
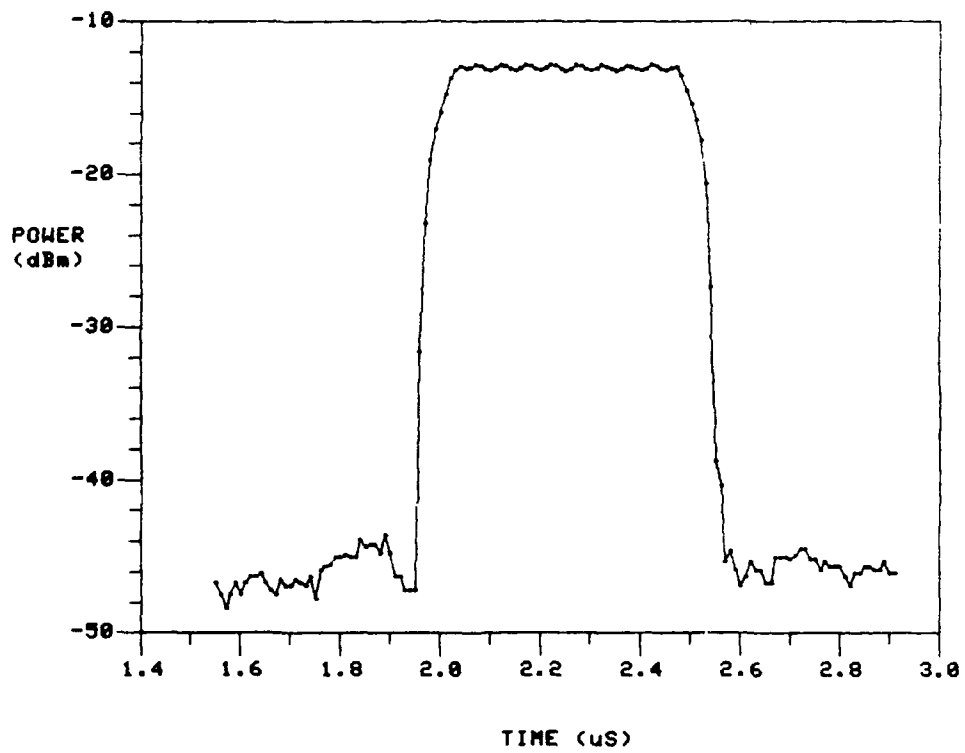


Fig. 19 Normalized Cross-Covariance Versus Input SNR  
Using Simulated Data ( Noise Bandwidth = 40 MHz )



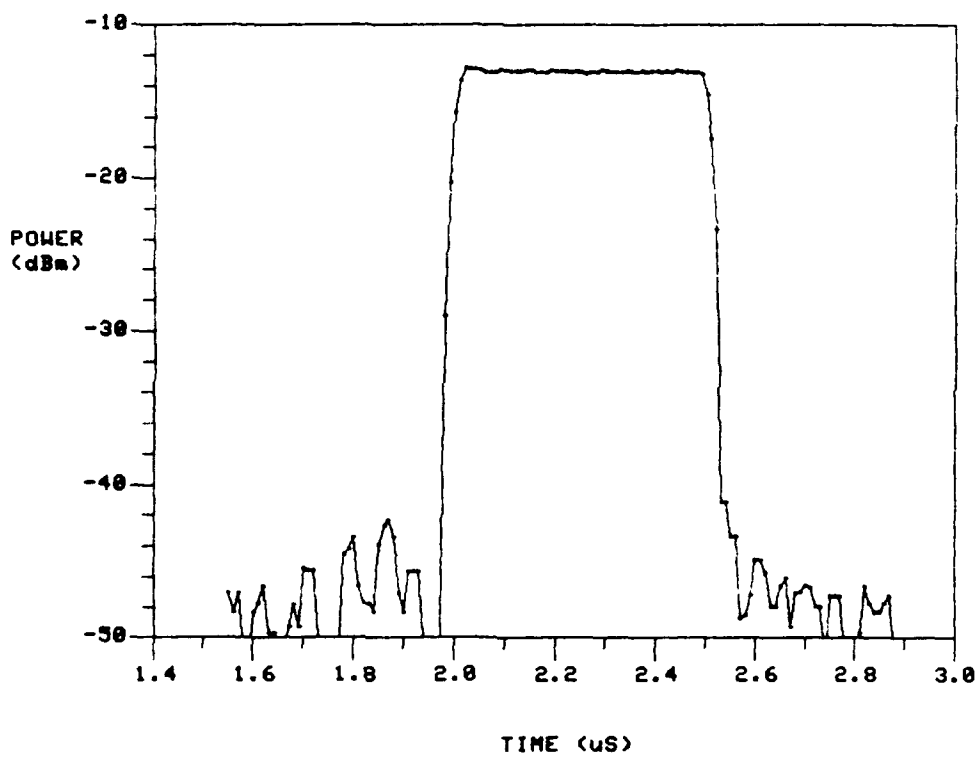
(a) Raw Data

Fig. 20 Envelope of a 0.5- $\mu$ s Pulse  
(Baseband Frequency = 40 MHz and  $T_s = 10$  ns)



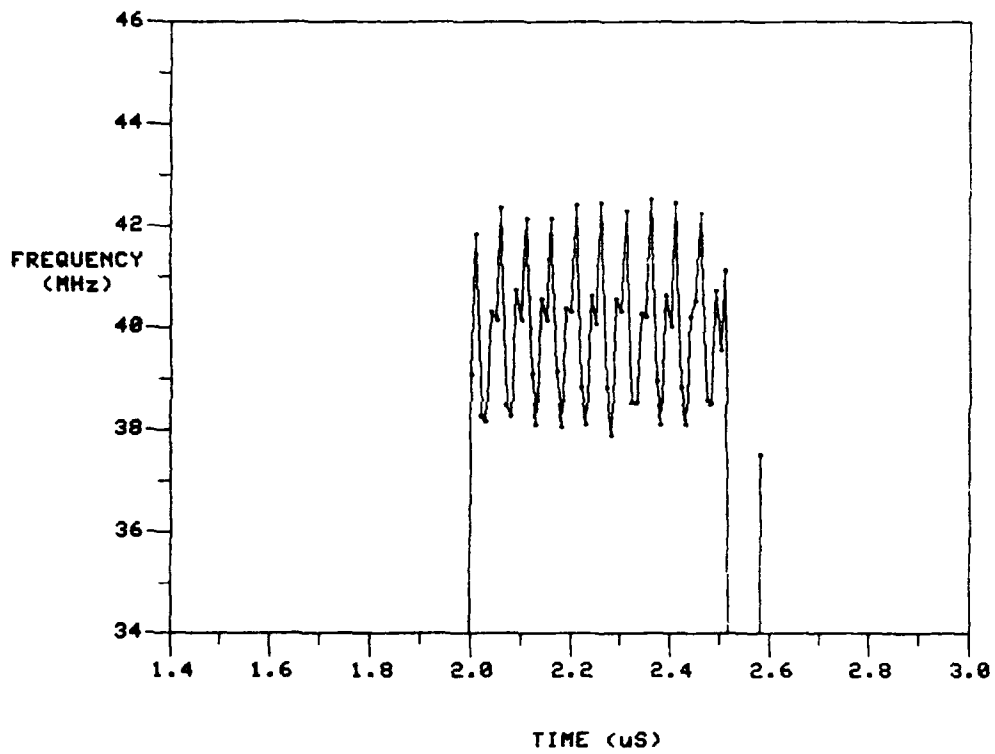
(b) After a 7-point Moving Average

Fig. 20 Instantaneous Frequency of a 0.5- $\mu$ s Pulse  
(Baseband Frequency = 40 MHz and  $T_s = 10$  ns)



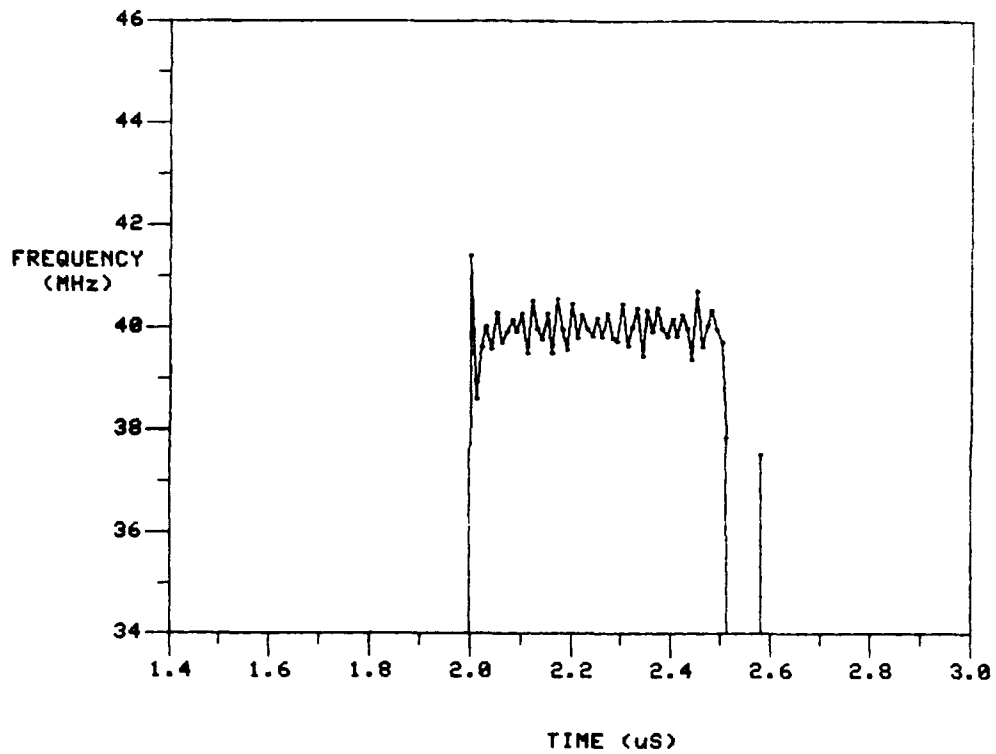
(c) After Compensation and 3-point Moving Average

Fig. 20 Envelope of a 0.5- $\mu$ s Pulse  
 (Baseband Frequency = 40 MHz and  $T_s = 10$  ns)



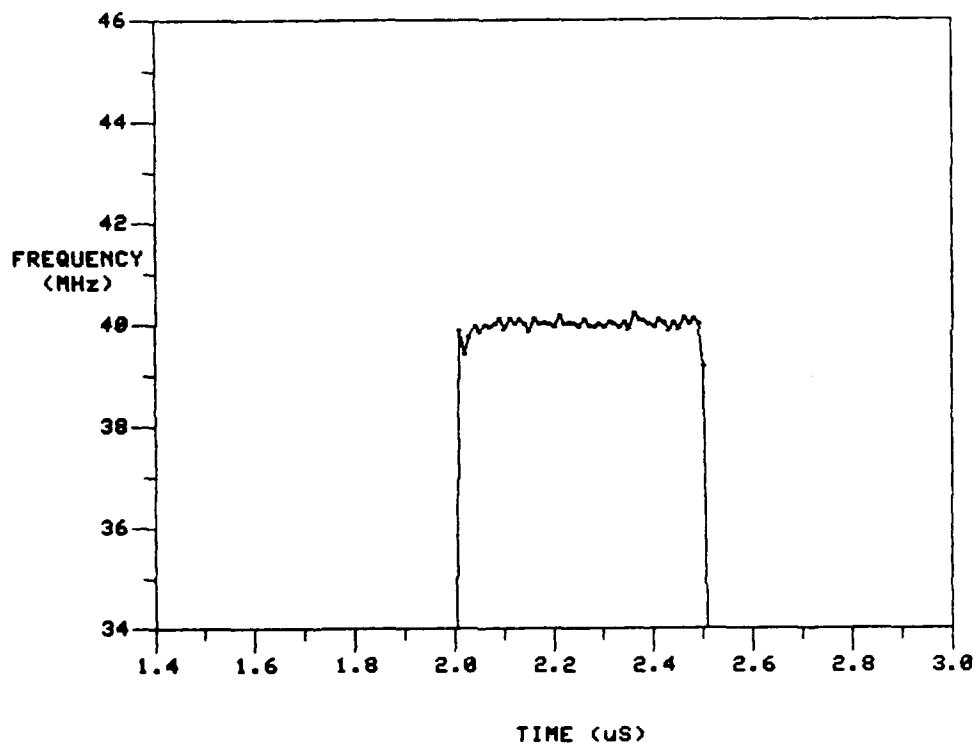
(a) Raw Data

Fig. 21 Instantaneous Frequency of a  $0.5\text{-}\mu\text{s}$  Pulse  
(Baseband Frequency = 40 MHz and  $T_s = 10\text{ ns}$ )



(b) After Compensation

Fig. 21 Instantaneous Frequency of a 0.5- $\mu$ s Pulse  
 (Baseband Frequency = 40 MHz and  $T_s = 10$  ns)



(c) After Compensation and 3-point Moving Average

Fig. 21 Instantaneous Frequency of a 0.5- $\mu$ s Pulse  
(Baseband Frequency = 40 MHz and  $T_s = 10$  ns)

applied to the noise, the resultant noise RMS value is found to decrease as expected. When the moving average is increased from one sample to five contiguous samples, the RMS value of the noise is found to decrease by a factor of  $\approx (5)^{1/2}$ . On the other hand, the signal power is relatively unaffected. As a result, the output SNR improves as the number of samples used in the moving average is increased. This happens because when a moving average is applied, the effective video bandwidth of the I/Q network is reduced by approximately the square root of the number of samples used in the moving average. As long as the video bandwidth is larger than the video bandwidth of the signal, the measured envelope of the signal is not affected.

Figure 21 shows the instantaneous frequency distribution. The raw data shows that a peak-to-peak frequency deviation is about 4 MHz. When a 3-point moving average is used after compensation, the RMS instantaneous frequency error is reduced drastically to below 80 KHz. Other types of low-pass digital filters such as Butterworth and Chebyshev are also used on the compensated instantaneous frequency of the signal. However, they are found to introduce ringing and overshoot which significantly distort the instantaneous frequency.

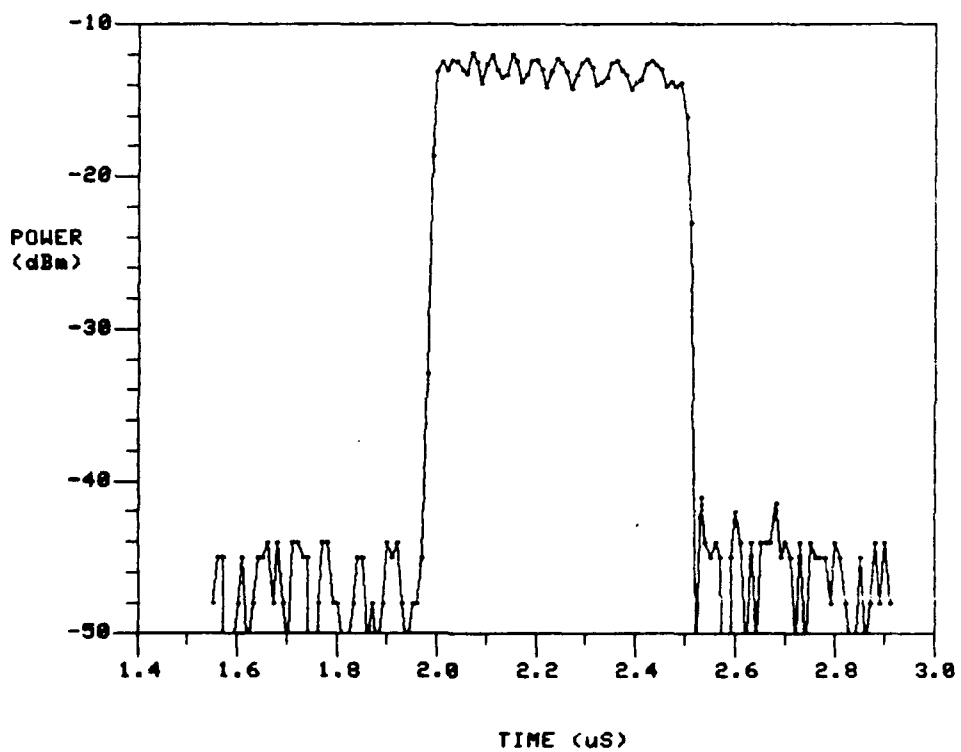
### 7.3.2 Linear FM Signal

A linear FM signal with a center frequency of 1960 MHz, and a frequency excursion of 10 MHz is applied to the I/Q network. The envelope and instantaneous frequency are shown in Figs. 22 and 23 respectively. It has the same pulse width and input SNR as for the pulsed signal. Even though the FM signal has a frequency excursion of 10 MHz, the same set of compensation parameters are used as if it were a CW signal centered at 1960 MHz. As can be seen from the plots, the compensated envelope and instantaneous frequency of the input signal have been reproduced accurately. In other words, the imbalance errors and DC offsets of the I/Q network are relatively insensitive to frequency variations. As a result, coarser frequency calibration steps can be used.

## 8.0 SUMMARY AND CONCLUSIONS

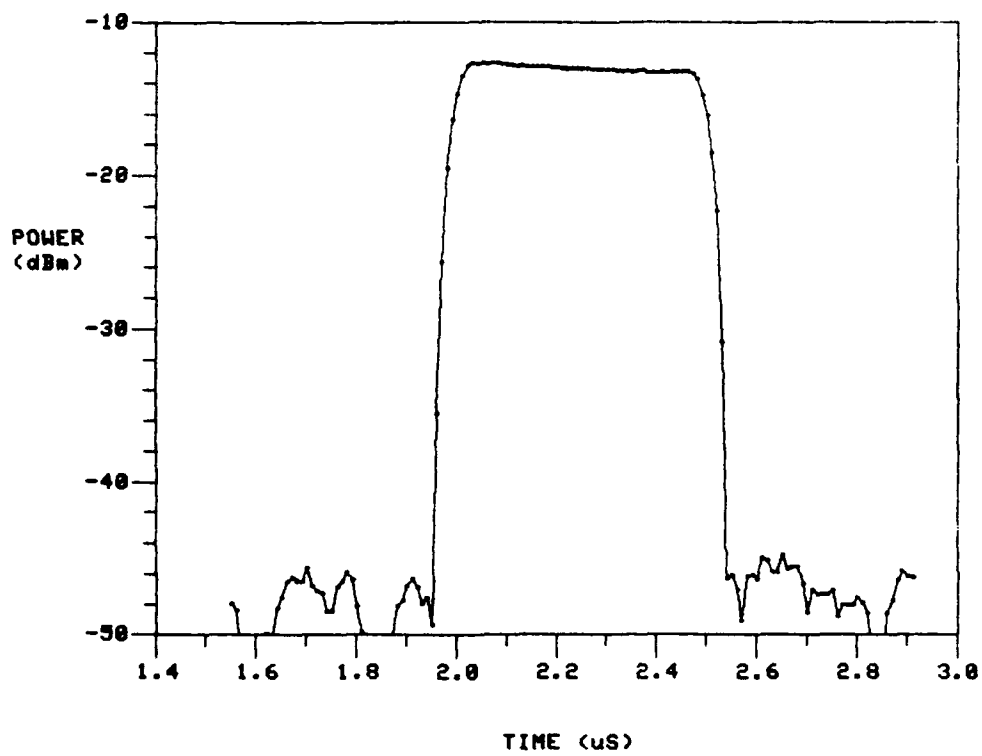
A simple in-phase/quadrature (I/Q) demodulator architecture which can measure the amplitude, phase and instantaneous frequency of radar signals has been examined in this report. By splitting the in-phase and quadrature components of the input signal using analog components, this architecture is potentially useful for radar ESM applications where wide instantaneous bandwidth and simple algorithms for extracting the modulation characteristics of radar signals are required. However, there are amplitude and phase imbalance errors and DC offsets in practical I/Q networks, which can introduce large systematic errors to the measurement. Two techniques, compensation and low-pass filtering using a moving average, have been proposed in this report for improving this simple architecture.

The effect of amplitude and phase imbalances and DC offsets is found to produce ripples on the measurement; the frequency of the ripples is harmonically related to the baseband frequency of the signal. For a given set of imbalance errors and DC offsets, the error introduced by the ripples on the instantaneous frequency is more severe and is directly proportional to the baseband frequency while the error is constant for both the amplitude and phase.



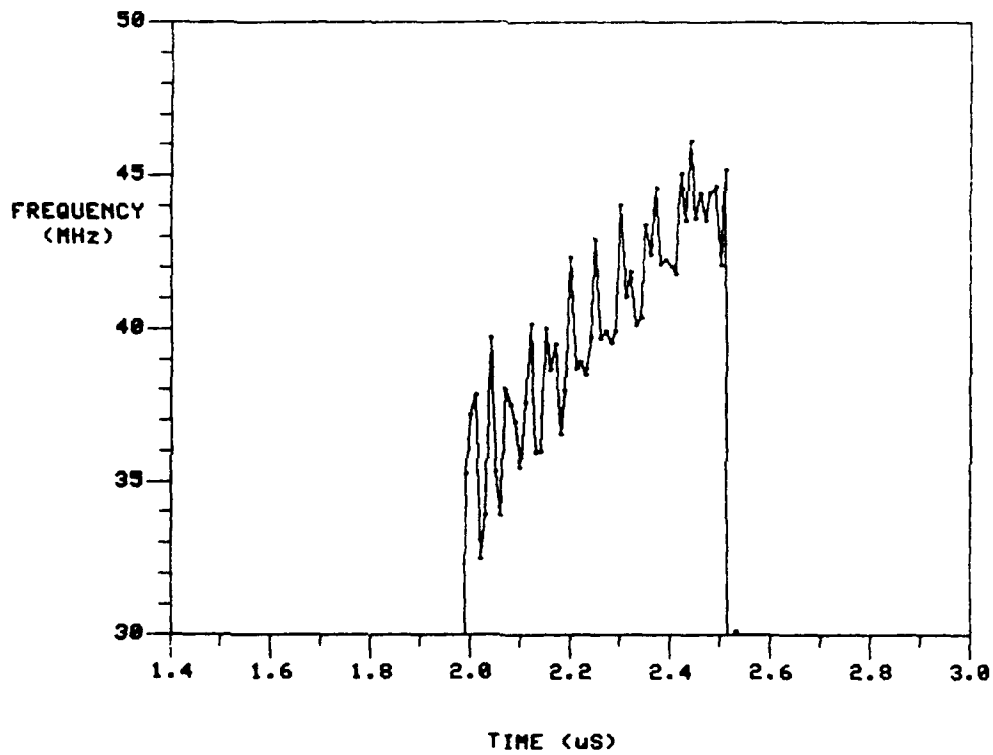
(a) Raw Data

Fig. 22 Envelope of a Linear FM Pulse  
(Pulse Width = 0.5 μs, Center Frequency = 40 MHz,  
 $\Delta f = 10$  MHz and  $T_s = 10$  ns)



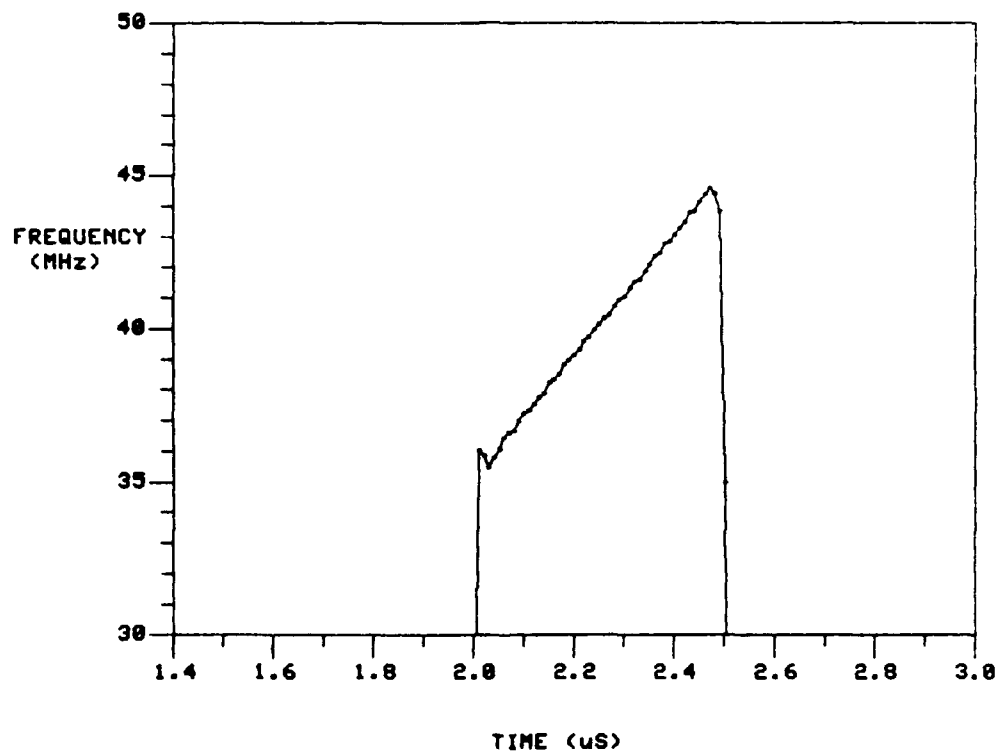
(b) After Compensation and 5-point Moving Average

Fig. 22 Envelope of a Linear FM Pulse  
(Pulse Width =  $0.5 \mu\text{s}$ , Center Frequency = 40 MHz,  
 $\Delta f = 10 \text{ MHz}$  and  $T_s = 10 \text{ ns}$ )



(a) Raw Data

Fig. 23 Instantaneous Frequency of a Linear FM Pulse  
(Pulse Width =  $0.5 \mu\text{s}$ , Center Frequency = 40 MHz,  
 $\Delta f = 10 \text{ MHz}$  and  $T_s = 10 \text{ ns}$ )



(b) After Compensation and 5-point Moving Average

Fig. 23 Instantaneous Frequency of a Linear FM Pulse  
( Pulse Width =  $0.5 \mu\text{s}$ , Center Frequency = 40 MHz,  
 $\Delta f = 10 \text{ MHz}$  and  $T_s = 10 \text{ ns}$ )

Some I/Q networks have been evaluated and the mean imbalance errors and DC offsets over a large frequency range can be large. In order to keep the systematic errors small, some form of compensation is needed to remove the mean errors and offsets. Once the mean errors and offsets are eliminated, the residual RMS errors as a function of frequency and input power level are quite small. If further improvement is required, a calibration dependent on frequency and input power level may be needed.

The measurement accuracy on the amplitude, phase and instantaneous frequency has also been analyzed and given in terms of input SNR. For large input SNR, the standard deviation of the phase error decreases inversely proportional to the square root of the input SNR while the standard deviation of the envelope remains constant as the input signal level is varied.

There are two basic functions performed by using a moving average. The effective noise bandwidth of the I/Q network can be reduced with no appreciable degradations to the signal of interest, with consequent improvement of the output SNR. The ripples produced by the imbalance errors and DC offsets are usually outside the video bandwidth of the signal of interest and thus can be reduced by low-pass filtering. In addition, a moving average is easy to implement digitally and does not introduce distortions such as ringing and overshoot.

Both the techniques of compensation and low-pass filtering using a moving average have been successfully demonstrated on the demodulation of pulsed and linear FM signals. They have been shown to be effective for improving the output signal-to-noise ratio and reducing systematic errors.

## 9.0 REFERENCES

- [1] J.B.Y. Tsui, *Digital Microwave Receivers*, Artech House Inc., Norwood, MA, 1989.
- [2] D.L. Sharpin, J.B.Y. Tsui, and J. Hedge, "The Effects of Quadrature Sampling Imbalances on a Phase Difference Analysis Technique", *Proceedings of the IEEE, National Aerospace and Electronics Conference, NAECON 1990, Vols. 1-3*; pp. 962-968, New York.
- [3] S.J. Goldman, "Understanding the Limits of Quadrature Detection", *Microwave & RF*, Dec, 1986.
- [4] J.P.Y. Lee, "I/Q Demodulation: Time-domain Analysis on Systematic Errors", to be published.
- [5] E. Oran Brigham, *The Fast Fourier Transform*, Prentice-Hall, Inc. Englewood Cliffs, New Jersey, 1974.
- [6] A. Papoulis, *Probability, Random Variables, and Stochastic Processes*, McGraw-Hill Inc., 1965.
- [7] A.V. Oppenheim and R.W. Schaffer, *Discrete-time Signal Processing*, Prentice Hall, Englewood Cliffs, New Jersey, 1989.
- [8] W.J. Lucas, "Tangential Sensitivity of a Detector Video System with R.F. Pre-amplification", *Proc. IEE*, Vol. 113, No.8, pp. 1321-1330, August 1966.
- [9] D. E. Johnson, *Introduction to Filter Theory*, Prentice-Hall, Inc. Englewood Cliffs, New Jersey, 1976.
- [10] H. Taub and D.L. Schilling, *Principles of Communication Systems*, McGraw-Hill Book Company, 1971.

SECURITY CLASSIFICATION OF FORM  
(highest classification of Title, Abstract, Keywords)

## DOCUMENT CONTROL DATA

(Security classification of title, body of abstract and indexing annotation must be entered when the overall document is classified)

|  |  |   |  |
|--|--|---|--|
| 1. ORIGINATOR (the name and address of the organization preparing the document. Organizations for whom the document was prepared, e.g. Establishment sponsoring a contractor's report, or tasking agency, are entered in section 8.)<br>NATIONAL DEFENCE<br>DEFENCE RESEARCH ESTABLISHMENT OTTAWA<br>SHIRLEY BAY, OTTAWA, ONTARIO K1A 0K2 CANADA   |  | 2. SECURITY CLASSIFICATION<br>(overall security classification of the document including special warning terms if applicable)<br><br>UNCLASSIFIED |  |
| 3. TITLE (the complete document title as indicated on the title page. Its classification should be indicated by the appropriate abbreviation (S,C or U) in parentheses after the title.)<br>I/Q DEMODULATION OF RADAR SIGNALS WITH CALIBRATION AND FILTERING (U)   |  |   |  |
| 4. AUTHORS (Last name, first name, middle initial)<br><br>LEE, JIM P.  |  |   |  |
| 5. DATE OF PUBLICATION (month and year of publication of document)<br>DECEMBER 1991  | 6a. NO. OF PAGES (total containing information. include Annexes, Appendices, etc.)<br>64 | 6b. NO. OF REFS (total cited in document)<br>10   |  |
| 7. DESCRIPTIVE NOTES (the category of the document, e.g. technical report, technical note or memorandum. If appropriate, enter the type of report, e.g. interim, progress, summary, annual or final. Give the inclusive dates when a specific reporting period is covered.)<br><br>DREO REPORT   |  |   |  |
| 8. SPONSORING ACTIVITY (the name of the department project office or laboratory sponsoring the research and development. Include the address.)<br>NATIONAL DEFENCE<br>DEFENCE RESEARCH ESTABLISHMENT OTTAWA<br>SHIRLEY BAY, OTTAWA, ONTARIO K1A 0K2 CANADA   |  |   |  |
| 9a. PROJECT OR GRANT NO. (if appropriate, the applicable research and development project or grant number under which the document was written. Please specify whether project or grant)<br><br>011LB11  |  | 9b. CONTRACT NO. (if appropriate, the applicable number under which the document was written)   |  |
| 10a. ORIGINATOR'S DOCUMENT NUMBER (the official document number by which the document is identified by the originating activity. This number must be unique to this document.)<br><br>DREO REPORT 1119   |  | 10b. OTHER DOCUMENT NOS. (Any other numbers which may be assigned this document either by the originator or by the sponsor)                       |  |
| 11. DOCUMENT AVAILABILITY (any limitations on further dissemination of the document, other than those imposed by security classification)<br><br><input checked="" type="checkbox"/> Unlimited distribution<br><input type="checkbox"/> Distribution limited to defence departments and defence contractors; further distribution only as approved<br><input type="checkbox"/> Distribution limited to defence departments and Canadian defence contractors; further distribution only as approved<br><input type="checkbox"/> Distribution limited to government departments and agencies; further distribution only as approved<br><input type="checkbox"/> Distribution limited to defence departments; further distribution only as approved<br><input type="checkbox"/> Other (please specify): |  |   |  |
| 12. DOCUMENT ANNOUNCEMENT (any limitation to the bibliographic announcement of this document. This will normally correspond to the Document Availability (11). However, where further distribution (beyond the audience specified in 11) is possible, a wider announcement audience may be selected.)  |  |   |  |

13. ABSTRACT ( a brief and factual summary of the document. It may also appear elsewhere in the body of the document itself. It is highly desirable that the abstract of classified documents be unclassified. Each paragraph of the abstract shall begin with an indication of the security classification of the information in the paragraph (unless the document itself is unclassified) represented as (S), (C), or (U). It is not necessary to include here abstracts in both official languages unless the text is bilingual).

(U) A simple in-phase/quadrature (I/Q) demodulator architecture which can measure the amplitude, phase and instantaneous frequency of radar signals is examined in this report. This architecture has a potential for radar ESM applications where wide instantaneous bandwidth and simple algorithms for extracting the modulation characteristics of radar signals are required. This I/Q architecture can meet the requirement by splitting an incoming signal into its in-phase and quadrature components using analog circuitries. However in practice, there are amplitude and phase imbalances between the two components and DC offsets, which can introduce large systematic errors to the measurement. In this report, we present novel techniques which can greatly reduce the systematic errors and improve the accuracy of the measurement. A time-domain analysis on the systematic errors is given. A calibration technique which can be used to correct for the imbalances and offsets is discussed. The effect of noise on the accuracy of the measurement is also examined. Imbalance errors and DC offsets of I/Q networks are measured and analyzed. Finally, a post-processing technique employing moving averages, which is shown to be effective for improving the output signal-to-noise ratio and reducing systematic errors, is also presented.

14. KEYWORDS, DESCRIPTORS or IDENTIFIERS (technically meaningful terms or short phrases that characterize a document and could be helpful in cataloguing the document. They should be selected so that no security classification is required. Identifiers, such as equipment model designation, trade name, military project code name, geographic location may also be included. If possible keywords should be selected from a published thesaurus. e.g. Thesaurus of Engineering and Scientific Terms (TEST) and that thesaurus-identified. If it is not possible to select indexing terms which are Unclassified, the classification of each should be indicated as with the title.)

I/ Q DEMODUALTION  
RADAR ESM  
DIGITAL RECEIVER  
RADAR SIGNAL PARAMETER MEASUREMENT